ADVANCED FUNCTIONAL MATERIALS
www.afm-journal.de

Innovations in Tactile Sensing: Microstructural Designs for Superior Flexible Sensor Performance

Guancheng Wu, Xiang Li, Rongrong Bao, and Caofeng Pan**

Tactile sensors have garnered considerable interest for their capacity to detect and quantify tactile information. The incorporation of microstructural designs into flexible tactile sensors has emerged as a potent strategy to augment their sensitivity to pressure variations, thereby enhancing their linearity, response spectrum, and mechanical robustness. This review underscores the imperative for progress in microstructured flexible tactile sensors. Subsequently, the discourse transitions to the prevalent materials employed in the fabrication of sensor electrodes, encapsulation layers, and active sensing mediums, elucidating their merits and limitations. In-depth discussions are devoted to tactile sensors adorned with microstructures, including but not limited to, micropyramids, microhemispheres, micropillars, microporous configurations, microcracks, topological interconnections, multilevel constructs, random roughness, biomimetic microstructures inspired by flora and fauna, accompanied by exemplar studies from each category. Moreover, the utility of flexible tactile sensors within the realm of intelligent environments is explicated, highlighting their application in the monitoring of physiological signals, the detection of sliding motions, and the discernment of surface textures. The review culminates in a critical examination of the paramount challenges and predicaments that must be surmounted to further the development and enhance the functional performance of tactile sensors, paving the way for their integration into advanced sensory systems.

1. Introduction

Sensor network technology has greatly transformed our daily lives and has significantly promoted the development of artificial intelligence,[1–5] human–computer interaction,[6–9] and other fields[10–18] as an emerging industry, bringing further improvements in efficiency, convenience, as well as safety and reliability for users. Within the realm of human interaction with the material world, tactile is one of the most common forms of sensory perception. Therefore, tactile sensors are extensively researched for their ability to detect physical stimuli like pressure and vibration,[19,20] translating them into electrical signals that can be conveniently interpreted by electronic systems.[21,22] However, traditional pressure sensors are typically rigid,[23–27] lacking flexibility and stretchability,[28] making it difficult for them to conform to curved interfaces. This limitation restricts their further application in wearable devices and machine tactile sensing fields.

The emergence of flexible tactile sensors has greatly solved these issues.[29] However, there is a growing need for enhanced sensor performance and dependability with the advance of flexible tactile sensors. Sensitivity and linearity response range are the most common bottlenecks encountered in in creating advanced flexible sensors, which still limit its better sensing performance and wider application scenarios.

The development of new materials can gradually break through the limitations of sensitivity and linearity. However, the research and development of new materials are often slow and challenging, so the researchers naturally began to consider making improvements using existing materials. To enhance sensitivity and linearity while using existing materials, the application of microstructures is one of the best options. By utilizing micro-level structural design, flexible tactile sensors can respond more sensitively to changes in pressure and improve their linearity. The use of these microstructures not only boosts the functionality of flexible tactile sensors but also broadens their potential applications across different industries.

In this review, we highlight the latest advancements in tactile sensors with microstructures (**Figure 1**). The first section briefly introduces four working mechanisms for tactile sensing and the commonly used materials for the substrate layers, electrodes, and

G. Wu, R. Bao, C. Pan
CAS Center for Excellence in Nanoscience
Beijing Key Laboratory of Micro-nano Energy and Sensor
Beijing Institute of Nanoenergy and Nanosystems
Chinese Academy of Sciences
Beijing 101400, China
E-mail: baorongrong@binn.cas.cn; pancaofeng@buaa.edu.cn
G. Wu, R. Bao, C. Pan
School of Nanoscience and Engineering
University of Chinese Academy of Sciences
Beijing 100049, China
X. Li, C. Pan
Institute of Atomic Manufacturing
Beihang University
Beijing 100191, China

The ORCID identification number(s) for the author(s) of this article can be found under https://doi.org/10.1002/adfm.202405722

DOI: 10.1002/adfm.202405722

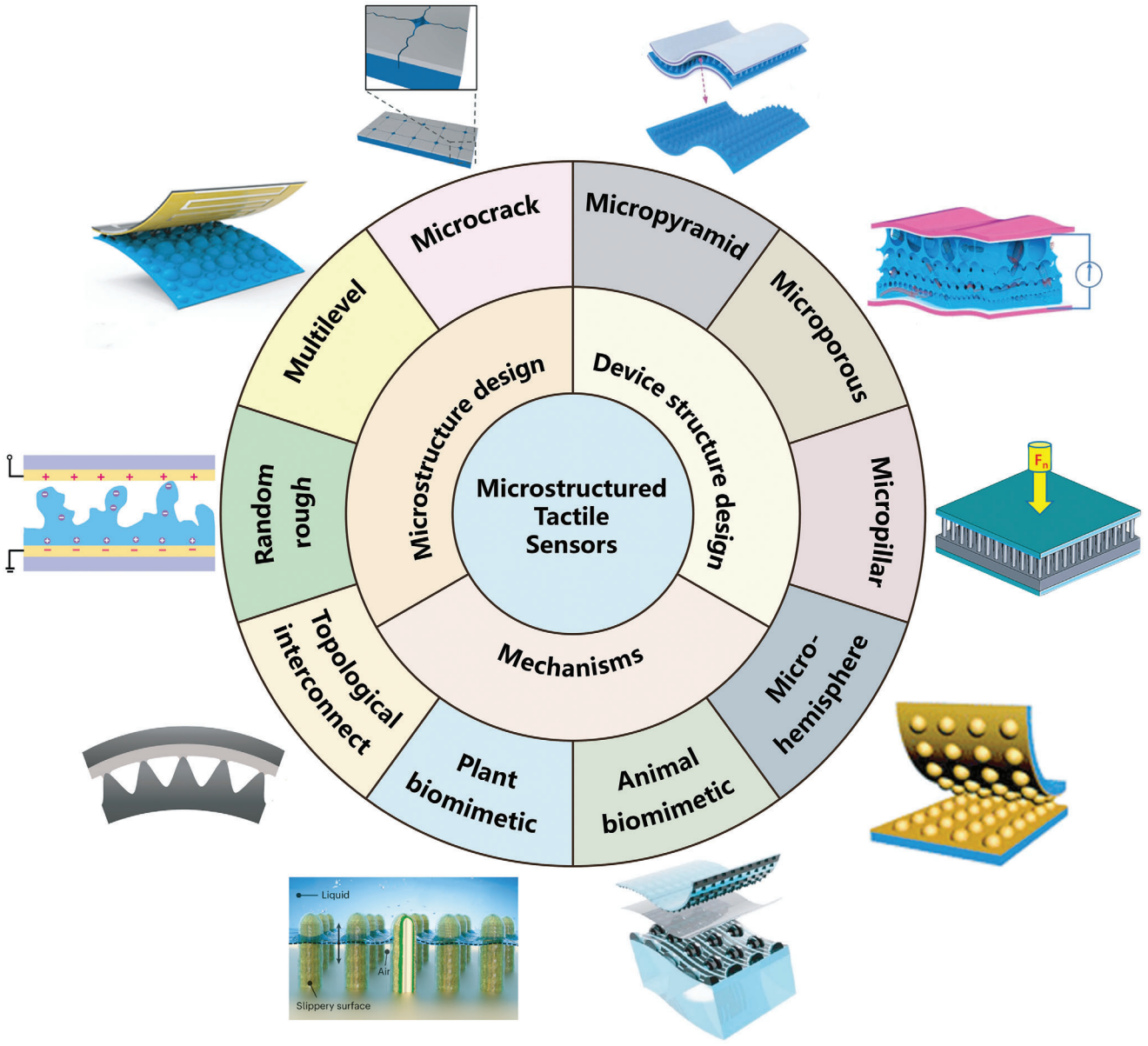

Figure 1. Overview of flexible pressure sensors focusing on mechanisms, device structure design, and microstructure design. Micropyramids: Reproduced with permission.[30] Copyright 2020, Wiley-VCH. Microhemispheres: Reproduced with permission.[31] Copyright 2018, The Royal Society of Chemistry. Micropillars: Reproduced with permission.[32] Copyright 2016, MDPI. Microporous structures: Reproduced with permission.[33] Copyright 2022, Elsevier. Microcracks: Reproduced with permission.[34] Copyright 2017, Springer Nature. Topological interconnections: Reproduced with permission.[35] Copyright 2022, Springer Nature. Multilevel structures: Reproduced with permission.[36] Copyright 2022, Wiley-VCH. Random roughness: Reproduced with permission.[37] Copyright 2020, Springer Nature. Animal bionic microstructures: Reproduced with permission.[38] Copyright 2018, AAAS. Plant bionic microstructures: Reproduced with permission.[39] Copyright 2023, Springer Nature.

active layers, as well as the required structure design for high sensor performance in flexible piezoresistive and piezocapacitive tactile sensors. The second section provides a detailed introduction to ten commonly used microstructures in tactile sensors and their representative works, analyzing their respective advantages and shortcomings. The third section introduces the three expanded application scenarios of microstructured tactile sensors in recent years, including physiological signal detection, sliding detection, and roughness perception. Finally, we summarize the development of flexible microstructured tactile sensors, addressing crucial issues and obstacles that need to be overcome for sensors with better performances.

2. Device Structure Design

Flexible tactile sensors typically consist of substrate layers, electrode layers, and active layers. The commonly used sensing mechanisms in flexible tactile sensors include piezoresistive,

piezocapacitive, piezoelectric, and triboelectronic. In this section, we will separately introduce the commonly used materials for the substrate layers, electrodes, and active layers, as well as the required structure design for high sensor performance for different sensing mechanisms.

Piezoresistive sensors detect pressure by monitoring the resistance shift when the active layer undergoes deformation. The piezoresistive active layer is typically composed of an elastic substrate with conductive fillers or intrinsic conductive polymers. It is often positioned between a set of interlocked electrodes or sandwiched between a pair of top and bottom electrodes. When a normal force is exerted, the contact resistance alters as a result of the expansion in the contact area or the permeation effect. Piezoresistive sensors have advantages such as simple manufacturing, easy control of device performance, simple signal readout mechanism, and high spatial resolution.[40] However, because of the thermal expansion of conductive polymers and the temperature-dependent nature of the resistivity of conductive fillers, resistive sensors experience significant resistance drift when exposed to temperature fluctuations, thereby restricting their effectiveness in environments with varying temperatures.

Piezocapacitive sensors typically consist of a set of top and bottom electrodes separated by a dielectric layer. The capacitance (C) of a capacitor is given by the formula $C = \epsilon A/d$, where ϵ is the dielectric constant, A is the effective area of the capacitor, and d is the separation distance between the electrodes. With the exertion of normal force, the adjustment in the distance d between the electrodes causes a shift in capacitance. The sensitivity of the capacitor can be adjusted by manipulating the material composition and structural configuration of the dielectric layer. Special electrode configurations can be utilized to amplify the variations in both the effective area (A) and the electrode distance (d) in response to the normal force. Piezoapacitive sensors offer benefits like reduced power usage and high durability. However, they often have poor immunity to interference, and variations in the surrounding environment can significantly impact their output signals, often requiring complex filtering circuits in practical applications.

Two additional mechanisms commonly used in sensors are piezoelectric and triboelectric. Piezoelectric sensors operate on the principle of the piezoelectric effect exhibited by certain materials such as polyvinylidene fluoride (PVDF),[41,42] poly[(vinylidenefluoride-co-trifluoroethylene] [P(VDF-TrFe)],[43] ZnO,[44] lead zirconate titanate (PZT),[45] piezoelectric gels,[46] and certain perovskites.[47,48] The exertion of pressure induces deformation in the piezoelectric material, leading to a shift in dipole density, and generating a piezoelectric voltage. Triboelectric sensors rely on the triboelectric effect and electrostatic interactions to sense pressure variations, typically using two rough surface layers with varying electronegativities to detect changes in pressure such as thermoplastic urethane (TPU),[49] polydimethylsiloxane (PDMS),[50,51] polytetrafluoroethylene (PTFE),[52] polyamide (PA),[53] PVDF[54] and silk.[55] With exertion and removal of the applied force, electric charges move between the layers, and neutralization of the charges on both sides is prevented because of the gap between them, leading to the creation of an immediate current in the external circuit. Since microstructures are seldom used in piezoelectric and triboelectric sensors, this article will primarily focus on the utilization of microstructures in piezoresistive and piezocapacitive sensors.

Conventional mainstream methods used to improve sensor performance include optimizing sensor materials,[56–58] optimizing sensor structures,[59–62] exploring new mechanisms,[63–66] and optimizing signal processing algorithms.[67–70] However, it is extremely difficult for material innovation or to further optimize the device structure, and optimizing signal processing algorithms cannot change the intrinsic flaws of the sensor. Based on the aforementioned reasons, utilizing microstructures can improve sensor performance just using existing materials. Therefore, the integration of microstructures into flexible tactile sensors has transformed the field of sensory technology by improving sensitivity and response capabilities. By incorporating microstructures into the design of sensor electrodes, active layers, and substrate layers, it is relatively easy to enhance the performance of sensors designed with existing materials and classical device structures.

The commonly used electrodes include top electrodes[71–73] and interdigital electrode[74,75] structures. In fact, many works involving microstructures have incorporated the microstructure design into the electrodes. For piezoresistive sensors, microstructured electrodes can enhance the contact zone of the electrode and the active layer when stress is exerted, causing a more significant change in the conductive path. For piezocapacitive sensors, microstructured electrodes can dramatically increase the capacitance area and reduce the electrode spacing, thus providing higher sensitivity. Sometimes designing the microstructure on the electrode layers can result in higher sensitivity and linear range increase compared to designing it on the active layers. For material selection, conductive polymers, metal materials, and carbon materials are generally used as electrodes.[76,77] Commonly used conductive polymer electrodes include polyaniline (PANI),[78,79] polythiophene (PEDOT:PSS),[80] PA,[81] polypyrrole (PPy),[82] etc., which have high conductivity and stability and are widely used in flexible tactile sensors. Traditional metal electrodes are mainly thin film electrodes of gold,[83,84] aluminum,[85] and copper,[86] which have good conductivity and mechanical strength but are relatively brittle and prone to breakage. In order to obtain stretchable and reliable metal electrodes based on nanostructures, silver nanowires,[87–89] gold nanowire networks,[90,91] liquid metal,[92] and other nanometallic materials[93–95] have been developed, which have excellent conductivity and flexibility and can maintain stable electrical performance when the sensor is bent and stretched. Commonly used carbon-based electrode materials include carbon black (CB),[96,97] graphene,[98,99] carbon nanotubes (CNTs),[100–103] etc., which are generally mixed into flexible polymers as composite electrode materials, such as PDMS, PU, etc. In addition, other inorganic materials such as indium tin oxide (ITO),[104,105] MXene,[106–112] and metal–organic framework (MOF)[113,114] also have similar application scenarios.

The active layer can be classified into a resistive layer for piezoresistive sensors and a dielectronic layer for the piezocapacitive layer, typically sandwiched between the electrodes. For piezoresistive devices, most of the resistive layers are made of polymers mixed with conductive materials,[115–123] and the material selection is similar to that of electrodes.[124–126] Some piezoresistive devices have abandoned the use of active layers and directly constructed the source of resistance change by

changing the conductive path between a pair of microstructured electrodes.[127] For capacitive devices, commonly used dielectric layer materials are usually elastic polymers such as Ecoflex,[128,129] PDMS,[130] PU,[131,132] silicone-based elastomers (SEs),[133] TPU,[134] poly(lactic-co-glycolic acid) (PLGA),[135] Poly(glycerol sebacate) (PGS),[136] poly(methyl methacrylate) (PMMA),[137] polyvinyl alcohol (PVA),[138] styrene-ethylene-butylene-styrene (SEBS),[139] and ion gels[140,141] based on these elastic polymers with higher dielectric constant such as PVDF-HFP/EMI:TFSI,[142] PU/[BMIm][BF_4],[143] PDMS/LiTFSI,[144] etc. In dielectric layer design, the dielectric layer either has microstructures with a high dielectric constant or is ultrathin in combination with microstructured electrodes, in order to make the capacitance change more significant.

The substrate layer is mainly used as the substrate for the bottom–up preparation of sensors and for packaging and protection after preparation. To fulfill the flexibility criteria of flexible sensors, the substrate material often necessitates low modulus, high flexibility, and high ductility. In specific application scenarios, it may also need to have characteristics such as water resistance,[145] breathability,[146,147] self-cleaning,[148] and biological compatibility.[149–151] Due to its adjustable modulus, controllable thickness, simple preparation, high chemical stability, and high transparency, PDMS is one of the most widely used substrate materials.[152–155] In addition, polymer films such as polyethylele (PE),[156] polyethylene terephthalate (PET),[157–159] Polyimide (PI),[160,161] PU, polyacrylonitrile (PAN), poly(L-lactide-co-ε-caprolactone) (PLCL),[162] polyethylene (PEN),[163,164] PVDF,[165] SEBS[166,167] and some traditional flexible fabrics[168] are also commonly used as substrate materials. With the continuous development of electrospinning technology, electrospun fiber films[169] such as PU, PVDF,[170] PAN, TPU,[116,171] and styreneic block copolymers (SBS), fluorinated ethylene propylene (FEP),[172] simultaneously provide ultrathin, breathability stretchability and intrinsic microstructure, which are widely researched and applied as a new generation of substrates.[173]

3. Microstructures

Microstructures refer to small-scale patterns or features integrated into the sensor design to improve its performance. Commonly used microstructures in flexible tactile sensors include micropyramids, microhemispheres, micropillars, microporous structures, microcracks, topological interconnections, multilevel structures, random roughness, and biomimetic structures inspired by animals and plants. These microstructures have been crucial in enhancing the sensor's sensitivity to subtle pressure changes, expanding the linear response range, and enhancing mechanical stability. By leveraging these innovative designs, researchers have been able to push the boundaries of tactile sensing technology. These innovative designs enable applications across various fields including robotics, prosthetics, healthcare, and human–computer interaction. As mentioned before, microstructures are generally designed on the electrodes or on the active layers. In this section, the aforementioned commonly used microstructures along with the representative works will be fully discussed, showing how microstructures improve sensors' performance.

3.1. Micropyramid Structures

In 2010, Bao and co-workers[174] pioneered the creation of a remarkably sensitive capacitive pressure sensor by integrating a dielectric layer with micropyramid structures. In 2014, Bao and co-workers[164] developed a skin-conformal sensor using micropillar structures for pulse signal amplification, a flexible pressure sensor using microhemisphere structures,[175] and a piezoresistive sensor based on hollow-sphere microstructures.[176] Since then, the four classic microstructure configurations, micropyramid, micropillar, microporous, and microhemisphere structures, have been established and have been extensively investigated in the use of microstructures in tactile sensors. Because of the limited compression area relative to the total expansion area and uneven stress distribution, stress becomes concentrated at the apex of the micropyramid structures, resulting in large structural deformations and higher sensitivity than devices without microstructures. Due to the aforementioned advantages and fabrication easiness, micropyramid structures have emerged as the most classic and extensively researched microstructures within the realm of tactile sensors.

For sensors with microstructures on the active layers, Tang and co-workers[177] fabricated a sandwich-structured capacitive tactile sensor by coating CNTs as electrodes and porous PDMS as dielectric layers on Ecoflex films with micropyramid microstructures. The sensor had a sensitivity of 2.51 kPa^{-1}, a detection limit of 2.0 Pa, a response speed of 84 ms, a wide response range of >10 kPa, and a high robustness of >5000 dynamic cycles. Yang and co-workers[178] synthesized piezocapacitive tactile sensors based on leakage-free polyelectrolyte elastomer with a micropyramid structure as the active layer with a sensitivity of 69.6 kPa^{-1}, a detection range of 1 MPa, and a fast response/recovery speed of 6 ms and good stability under either static or dynamic loads. Khademhosseini and co-workers[30] demonstrated a fully solution-processable transparent piezocapacitive tactile sensor with hydrogel methacryloyl (GelMA) micropyramid arrays as the core dielectric layer and PDMS/PEDOT:PSS/PDMS films as electrodes (**Figure 2a**). Contrasted with devices lacking microstructures, the sensor had a high-pressure sensitivity of 0.19 kPa^{-1} and a low detection limit of 0.1 Pa with a small hysteresis error of only 4%. Moreover, the hydrogel exhibited a durability of 3000 test cycles owing to its robust chemical bonds, along with 3-day stability facilitated by an encapsulation layer that hindered water evaporation. In addition to the commonly used inverted mold methods, Pan and co-workers[179] prepared versatile self-assembled electrospun micropyramid arrays (EMPAs) by electrospinning PVDF, and plated gold as an electrode to prepare a piezocapacitive tactile sensor (Figure 2b). The sensor demonstrated a sensitivity of 19 kPa^{-1}, a rapid response time of 0.8 ms, and an extremely low detection threshold of 0.05 Pa, enabling it to detect even the weight of mosquitoes. The device was ultralightweight, ultrathin, and breathable, with a thickness of only 47 µm with great robustness and bioaffinity. In order to eliminate the influence of strain in stress sensing, Wang and co-workers[180] designed a tensile piezocapacitive tactile sensor using PVDF-HFP/EMIM:TFSI/HMDA ionic elastomer and Ecoflex electrodes coated with silver nanoparticles (Figure 2c). The sensor exhibited a sensitivity of 4.5 kPa^{-1}, a response range of 10 kPa, and a minimal pressure detection threshold of 0.2 Pa while also

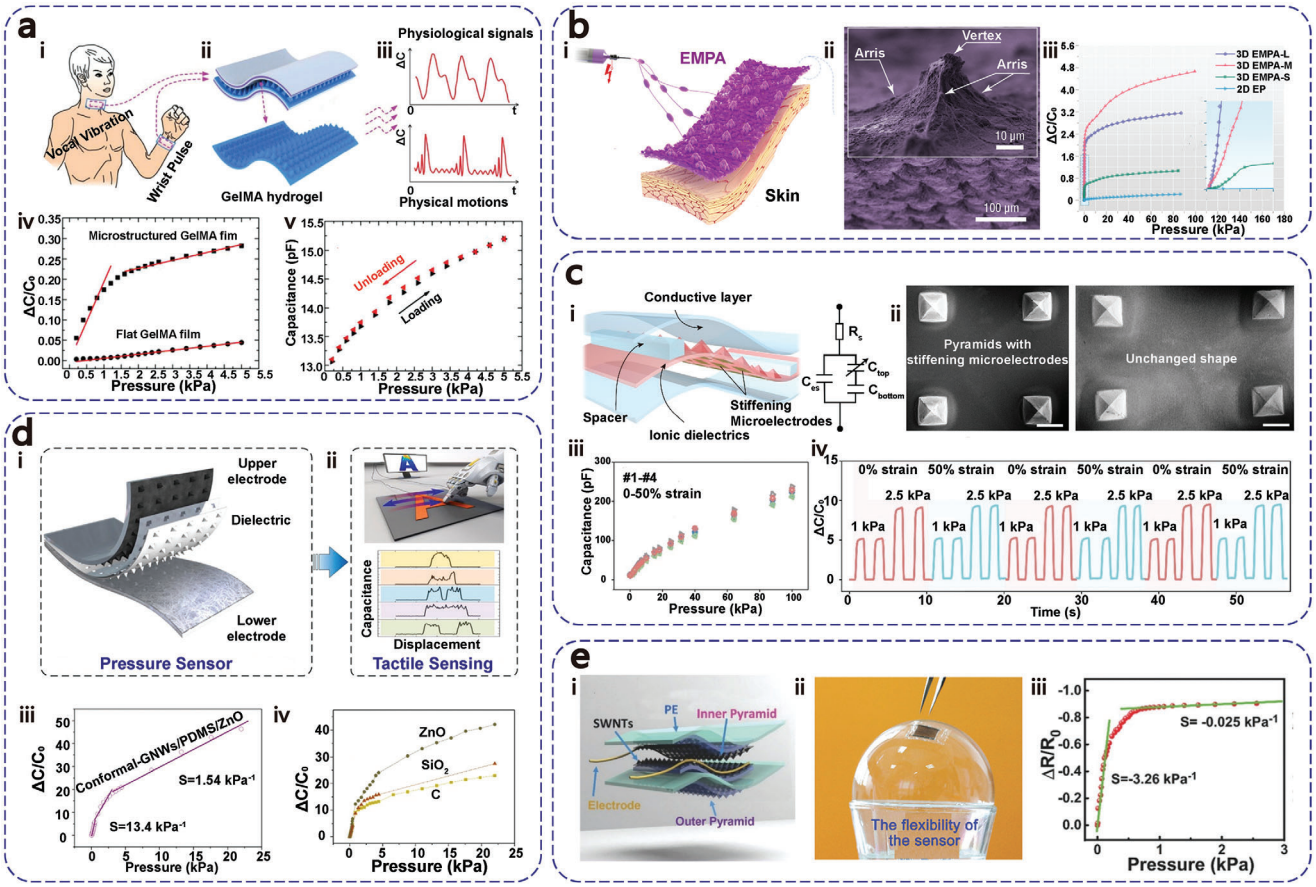

Figure 2. Sensors with micropyramid structures. a) i–iii: Diagram illustrating GelMA capacitive tactile sensor and its wearing applications. iv: Sensitivity compared with the device of flat GelMA dielectric layer. v: Capacitance variation during loading–unloading cycles. Reproduced with permission.[30] Copyright 2020, Wiley-VCH. b) i: Fabrication and structure of EMPAs. ii: SEM image of an EMPA. iii: Variation in capacitance when exerting pressure. Reproduced with permission.[179] Copyright 2019, Springer Nature. c) i: Structure of the sensor and its equivalent circuit. ii: SEM images of the microstructures at 0 & 50% strains. iii: Capacitance variations of four individually manufactured sensors under 0% & 50% strain iv: Consistency of the sensor performance during repeated pressure loading and stretching cycles under 0% & 50% strains. Reproduced with permission.[180] Copyright 2021, AAAS. d) i, ii: Illustration of the sensor and its application in slipping imaging. iii: Capacitance change and sensitivity under pressure. iv: Comparison of the effects of ZnO, SiO_2, and C film. Reproduced with permission.[182] Copyright 2021, Elsevier. e) i: Schematic configuration of the flexible tactile sensor. ii: Photo of the light-weight sensor on a gas bubble. iii: Resistance changes of the sensor in pressure change. Reproduced with permission.[183] Copyright 2018, Wiley-VCH.

remaining insensitive to strain up to 50%. The overall capacitance of the sensor was dominated by the electric double layer formed between the top of the pyramid and the top electrode, and the plane stretching did not affect the actual capacitance area, so the sensor could both maintain a remarkably stable capacitance value in situations with no pressure or under normal pressure. Cheng and co-workers[181] fabricated piezocapacitive tactile sensors with ultrawide linear range using PMMA/Au electrode with gradient micropyramid PMMA array and PVDF-HFP-based [EMI][TFSI] ionic liquid dielectric layer. The gradient micropyramid PMMA array was manufactured via programmable laser ablation. The sensor exhibited a sensitivity of 33.7 kPa^{-1} within an ultrawide linear range of 1700 kPa with excellent linearity (R^2 = 0.99), detection limit of 0.36 Pa, rapid response/recovery, and excellent repeatability.

For sensors with microstructures on the electrodes, Yang and co-workers[182] demonstrated a flexible piezocapacitive sensor featuring microstructured graphene nanofilms (GNWs) and a conformal microstructured dielectric layer comprising PDMS and the piezoelectric enhancer ZnO (Figure 2d). The piezoelectric sensor had an ultrahigh sensitivity of 22.3 kPa^{-1}, a fast response time of 25 ms, and a wide pressure range of 22 kPa. The capacitance of the sensor was further boosted by the polarized electric field created through the piezoelectric properties of the ZnO film. Furthermore, by combining the electrode and dielectric layer, the issue of slippage between the consecutive layers was resolved, leading to a notable enhancement in mechanical stability. In order to further expand the application scenarios of the sensor, Zhang and co-workers[183] used two SWNTs/PDMS/PE films with micropyramid structures to assemble an ultralight (17.6 mg), ultrathin (150 μm) piezoresistive flexible tactile sensor, which could be even placed on the surface of air bubbles (Figure 2e). The sensor had a sensitivity of 3.26 kPa^{-1} and a response range of 3 kPa with the capability of detecting changes in shear force caused by the dynamic interplay between the external micropyramid structure on the sensor and the surface of the

material to be measured and can detect microfringe sizes as low as 15 μm in width by detecting vibration.

3.2. Microhemisphere Structures

Microhemispherical structure is also one of the common structures in tactile sensors. The contact area of the hemisphere expands as the stress increases, which contributes to the enhanced performance of the devices. The microhemispherical structure has the capability to generate distinct deformations in response to different types and orientations of external forces, enabling it to recognize and distinguish various mechanical signals, including pressure, shear, bending, and torsional forces. However, compared with the micropyramid structure, the top of the hemisphere structure is almost flattened under high pressure, and it is difficult to obtain further increase in the electrode distance and contact area by enhancing stress, leading to a relatively small detection range and linear range.

For sensors with microstructures on the active layers, Shi and co-workers[184] obtained a piezocapacitive tactile sensor with a surface fold structure by using a Ni template to mold the PDMS into a uniform microhemisphere structure, pre-stretching the PDMS and plating it with gold. The device had a sensitivity of 0.382 kPa^{-1}, fast response and recovery times of 26 and 25 ms, respectively, and a minimum detection pressure of 4 Pa. Li and co-workers[185] fabricated piezoresistive tactile sensors with concave hemispherical microstructures by stainless steel ball molding. The sensor had a sensitivity of 27.97 kPa^{-1}, a detection limit of 0.5 Pa, a response/recovery time of 45 ms/35 ms, and a detection range of 460 KPa. Chen and co-workers[186] developed a fully soft piezocapacitive tactile sensor a striped film coated with MWNTs/PDMS as the electrode layer and a hemispherical elastomer composed of Ecoflex as the dielectric layer (**Figure 3a**). Combined with micro-ridge and microhemispherical dielectric structure, this sensing configuration facilitated the detection of forces from all directions under 10 kPa with a sensitivity of 0.306 kPa^{-1} and a wide response range of 2.55 Pa–160 kPa with a minimum detection limit of 10 mg (2.55 Pa). Pan and co-workers obtained a piezocapacitive transparent ion sensing (TIS) tactile sensor based on an ion–electron sensing mechanism by using a PDMS substrate to mold highly transparent ionic gel arrays with microhemisphere structures, and anti-reflection (AR) PET film sprayed with AgNWs ink as the electrode (Figure 3b). The devices incorporate ionic gels with varying densities of microhemispheric array, varying hemisphere diameters, and the maximum density of hemispheres across different feature sizes, indicating the highest device sensitivity of 83.9 kPa^{-1} with ultrahigh optical transparency of 96.9%.[187] In addition to the inverted mold method, Levkin and co-workers[188] fabricated a hemispherical gel-based piezocapacitive sensor using a hydrophilic array on a hydrophilic-treated aluminum substrate filled with hydrogel precursor solution. Compared to planar hydrogel devices, the sensor has experienced a notable enhancement in sensitivity. By further optimizing the topography of the sensor array, the sensor performed a high sensitivity of 0.29 kPa^{-1} and a response range of 100 kPa using an inhomogeneous conductive gel array.

For sensors with microstructures on the electrodes, Bhattacharjee and co-workers[189] prepared a piezoresistive tactile sensor utilizing a hemispherical microstructured PDMS film. Through comparative tests, sensors with a hemisphere radius of 100 μm on 0.5 mm thick substrates exhibited a sensitivity of 9.51 kPa^{-1} within 6 kPa, with and a detection range of 120 kPa. As the thickness of the substrate decreased, the sensitivity of the sensor improved, but the ability to detect large pressures decreased. featuring an interlocking design by casting a blend of PDMS elastomer and curing agent onto a PS mold with a microspherical array, and depositing gold nanoparticles on the surface of the prepared PDMS film by magnetron ion sputtering (Figure 3c). The sensor showed a sensitivity of 196 kPa^{-1} and a broad pressure sensing range of 0–100 kPa, along with exceptional capability such as a minimum detection threshold of 0.5 Pa, rapid response time of 26 ms, and excellent reversibility exceeding 10 000 cycles. The sensor could identify florets with a mass of 4.7 mg, equivalent to a static pressure of 0.5 Pa, and its response time was as short as 26 ms during the loading–unloading process.[31] Zhu and co-workers[190] fabricated flexible piezoresistive tactile sensors by sandwiching polypropylene nonwoven fabrics (PPNWFs) coated with CNTs between the microhemisphere PDMS layer and the interlock electrode (Figure 3d). could undergo additional compression at high pressures, the resistance of the fiber layer decreased consistently, resulting in a sensor that exhibited sensitive and continuous resistance changes in response to pressure. These pressure sensors demonstrated a high sensitivity of 6.3 kPa^{-1}, an extremely wide linear range from 4.6 Pa to 800 kPa, a quick response time of 72 ms, a relaxation time of 88 ms, and exceptional stability over 10 000 loading and unloading cycles at 127.4 kPa.

3.3. Micropillar Structures

Micropillar structure concentrates the applied stress on the pillar arrays, which can introduce greater deformation than the planar structure, resulting in a sharp increase in the conductive path of the piezoresistive sensor or a sharp decrease in the electrode distance of the piezocapacitive sensor, thus improving the sensitivity. The geometry of the micropillar arrays is uniform from the bottom to the top, so this type of sensor tends to have better linearity than micropyramid and hemispherical sensors.

For sensors with microstructures on the active layers, Lin and co-workers[32] molded MWCNT/PDMS into a Si template to explore the effects of different pillar sizes on stress sensitivity (**Figure 4a**). Obtained by Ar ion beam procedure to modify the surface texture of the micropillar, the piezoresistive tactile sensor showed its peak sensitivity of 21.7 kPa^{-1} and a response range of 25 kPa with a certain shear force detection ability. To further extend the sensor's response range, Xing and co-workers[191] obtained a capacitive tactile sensor with a gradient hollow micropillar array by inverting the PDMS dielectric layer into a PLA template (Figure 4c). The pressure was concentrated at the bottom of the micropillar, and the presence of air within the structure raises the compression challenge, expanding the sensing range of the tactile sensor. The sensor had a sensitivity of 0.636 kPa^{-1}, a linear sensing range of 8 Pa–500 kPa, a response time of 40 ms, and excellent repeatability and durability of 6000 cycles.

For sensors with microstructures on the electrodes, Guo and co-workers[192] reported piezocapacitive tactile sensors

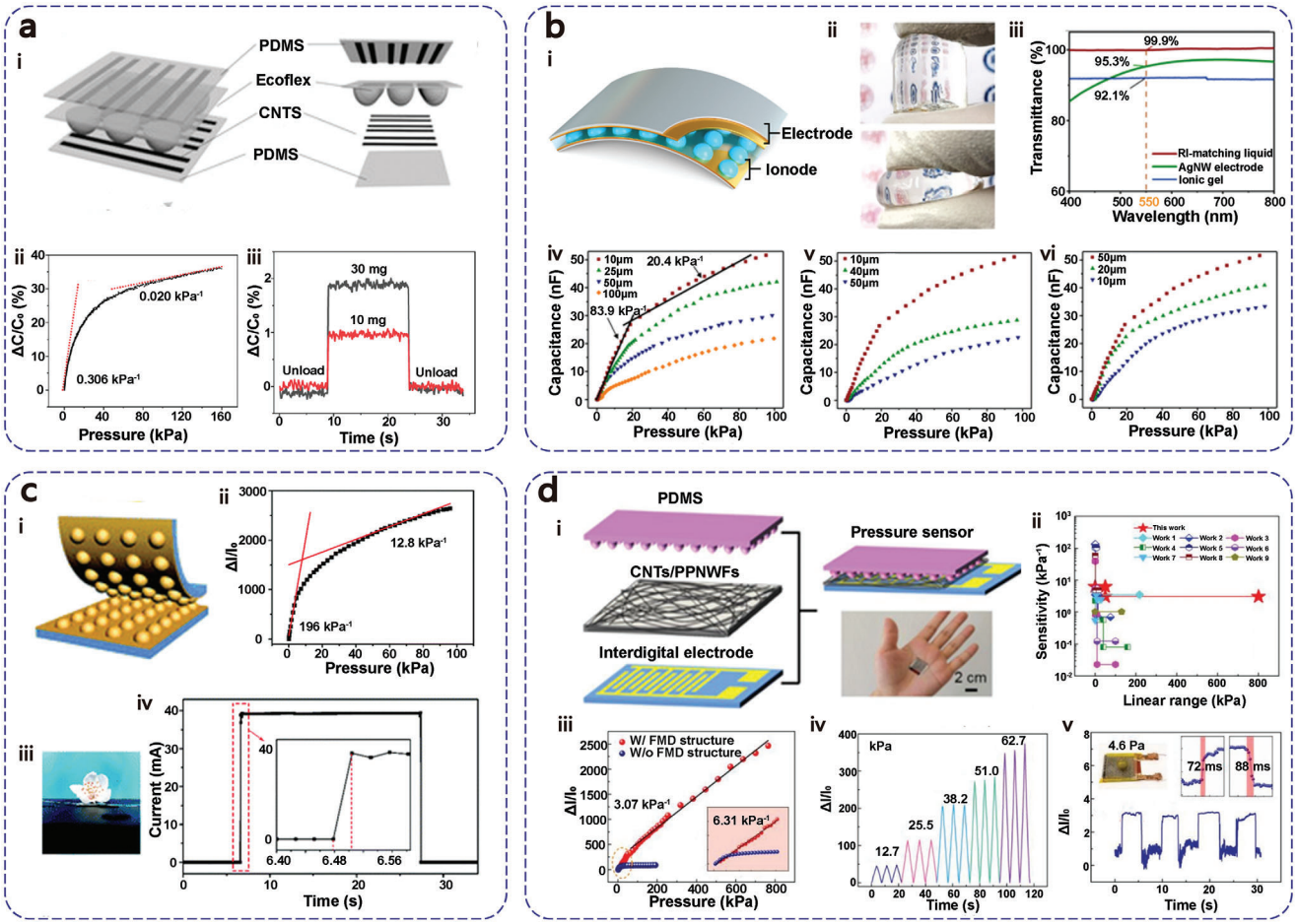

Figure 3. Sensors with microhemisphere structures. a) i: Schematic diagram of the sensor structure in perspective view. ii: Capacitance curve of the sensor under continuous pressure. iii: The optimized devices respond under micro pressures of 50 and 10 mg. Reproduced with permission.[186] Copyright 2022, MDPI. b) i: The structural illustration of the device. ii: The photos of the ionic gel indicate its high elasticity. iii: Visible spectrums of all the building materials of the devices. iv–vi: Graphs of the devices employing ionic gels with varying densities of hemisphere arrays, diverse hemisphere diameters, and maximum hemisphere density at different feature sizes, respectively. Reproduced with permission.[187] Copyright 2022, Springer Nature. c) i: Schematic illustration of the device. ii: Change in current in relation to applied pressure. iii: Electrical reaction to the placement of a small flower on the device. Reproduced with permission.[31] Copyright 2018, The Royal Society of Chemistry. d) i: Structure and applications of the designed FMD-structured flexible pressure sensors. ii: Comparison to other piezoresistive sensors. iii: Change in the relative current of the sensor with and without microhemisphere structure. iv: Responses to various low pressures. v: Dynamic reaction to loading/unloading a bean on the device. Reproduced with permission.[190] Copyright 2023, Wiley-VCH.

consisting of a PDMS micropillar array bottom electrode coated with Au, an ionic gel layer composed of P(VDF-HFP) [EMIM][TFSI] and a CPI film top electrode coated with Au (Figure 4d). The sensor exhibited high linearity ($R^2 = 0.999$) and sensitivity of 33.16 kPa^{-1} over a pressure range of 12–176 kPa with a detection limit of 0.9 Pa and a response time of 9 ms. The linear response was achieved by the post-buckling of the pillars in contact with the ionic gel under high pressures. In addition to the traditional counter electrode structure, Guo and co-workers[193] used the skin as a part of the sensor and a sensing electrode and counter electrode with a gold-plated PDMS micropillar array structure to attach to the human skin to form a skin-electrode piezocapacitive tactile sensor, which greatly simplifies the structure of the wearable tactile sensor (Figure 4b). The sensor exhibited a sensitivity of 11.8 kPa^{-1} and a response speed of 30 ms on the basis of good biocompatibility. It is worth noting that the dynamic tactile sensing performance remained unaffected by the distance between the electrodes and the stress applied to the counter electrodes.

3.4. Microporous Structures

Microporous structure is also one of the commonly used structures for microstructure sensors due to its ease of fabrication. Except for the template method, emulsion, autoclave foaming, freeze-drying, phase conversion, etc. are all methods for rapid preparation of microporous structures. Devices with porous dielectric structures concentrate stresses on the framework, leading to enhanced compressibility, rapid rebound rates, and an extended linear pressure range. Microporous structures allow the sensor to have ample room for elastic deformation under external pressure, providing a pressure sensing of more than tens of

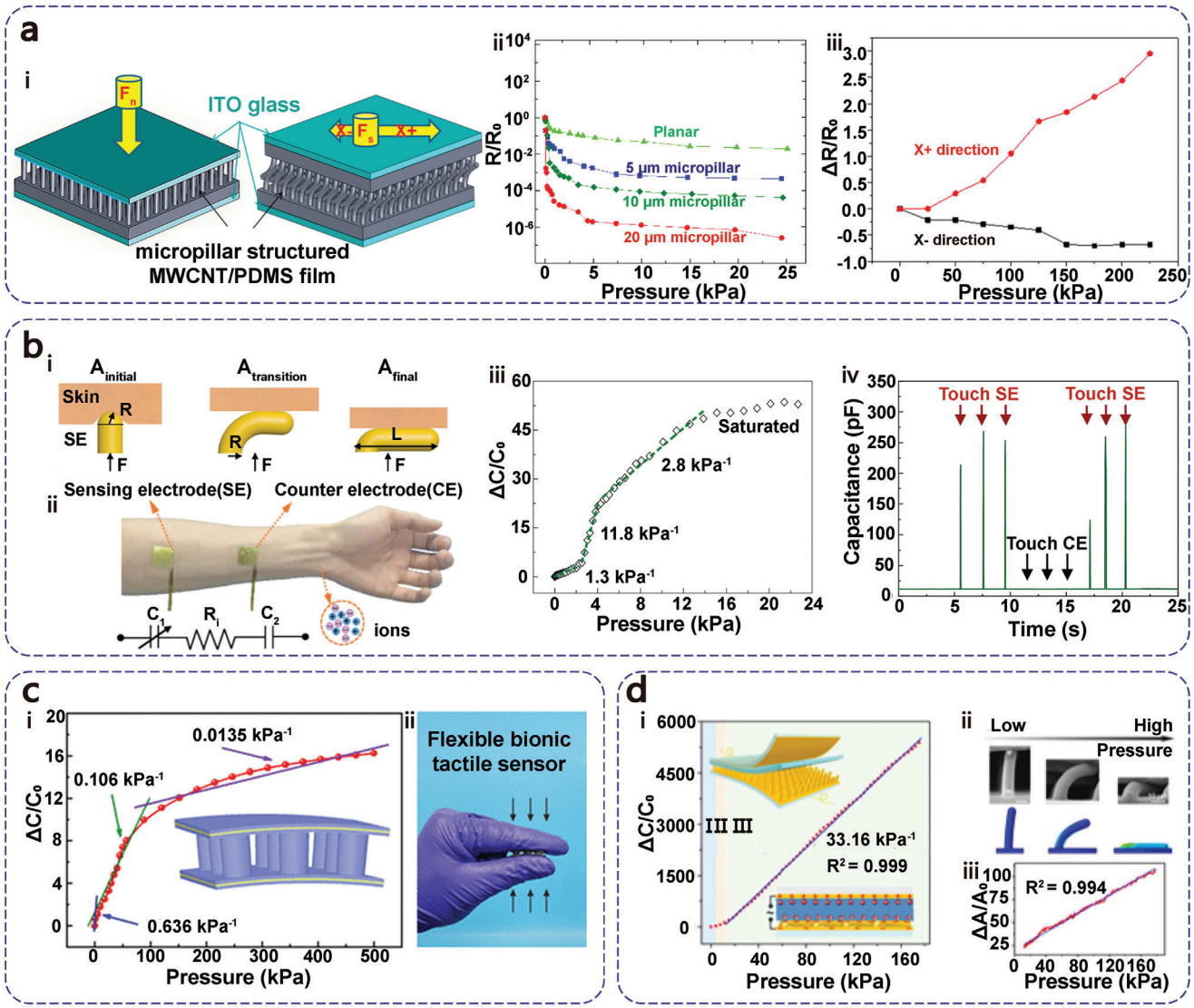

Figure 4. Sensors with micropillar structures. a) i: 3D schematics of the sensor. ii: Efficacy of micropillar with different heights. iii: Shear response of the sensor. Reproduced with permission.[32] Copyright 2016, MDPI. b) i: Illustrations showing the initial, transitional, and final pillar morphology. ii: Image showing the device with a sensing electrode (SE) and a counter electrode (CE) attached to the arm. iii: Capacitance change under pressure. iv: SE and CE tap reactions. Reproduced with permission.[193] Copyright 2021, Springer Nature. c) i: Relative capacitive change under pressure. ii: Photos showing the flexibility of the device. Reproduced with permission.[191] Copyright 2022, American Chemical Society. d) i: Capacitance change and device illustration. ii: SEM image of a micropillar and micropillar structure under different pressures. iii: Contact area variation under pressure. Reproduced with permission.[192] Copyright 2021, Elsevier.

kPa. The air volume fraction within the porous structure is very high, making the device light and well permeable, so the normal breathing and sweat excretion of the human skin are not affected. Microporous structure brings no obstruction to the regular functions of the human body, which is a good structure for the preparation of wearable tactile sensors with biological affinity.

Almost all porous microstructures are designed on the active layers of the sensors. Wong and co-workers[194] prepared highly ordered 3D porous graphene sponges (OPGSs) by emulsion method and created piezoresistive pressure sensors showing exceptional flexibility and sensitivity. OPGSs exhibited a highly ordered 3D structure with ultralow density, high porosity, and conductivity with a sensitivity of 1.46. Lee and co-workers[195] prepared a porous piezocapacitive sensor by applying a PDMS film onto PS beads arranged on a substrate, dissolving the beads, and transferring the film onto ITO/PET film. The sensor had a sensitivity of 0.63 kPa^{-1}, stability of 10 000 cycles, response and relaxation time of 40 ms, and detection limit of 2.42 Pa. Meng and co-workers[143] fabricated piezocapacitive tactile sensors by layering a porous PU/ionic liquid sponge between two electrospun TPU/MXene nanofiber electrodes. The sensor had a sensitivity of 105.77 kPa^{-1} and a detection range of 80 kPa with good air permeability, moisture permeability, and excellent heat dissipation capacity. Colin and co-workers[196] proposed a piezocapacitive sensor based on PDMS composite foam filled with conductive carbon black particles made by the water-in-oil emulsion

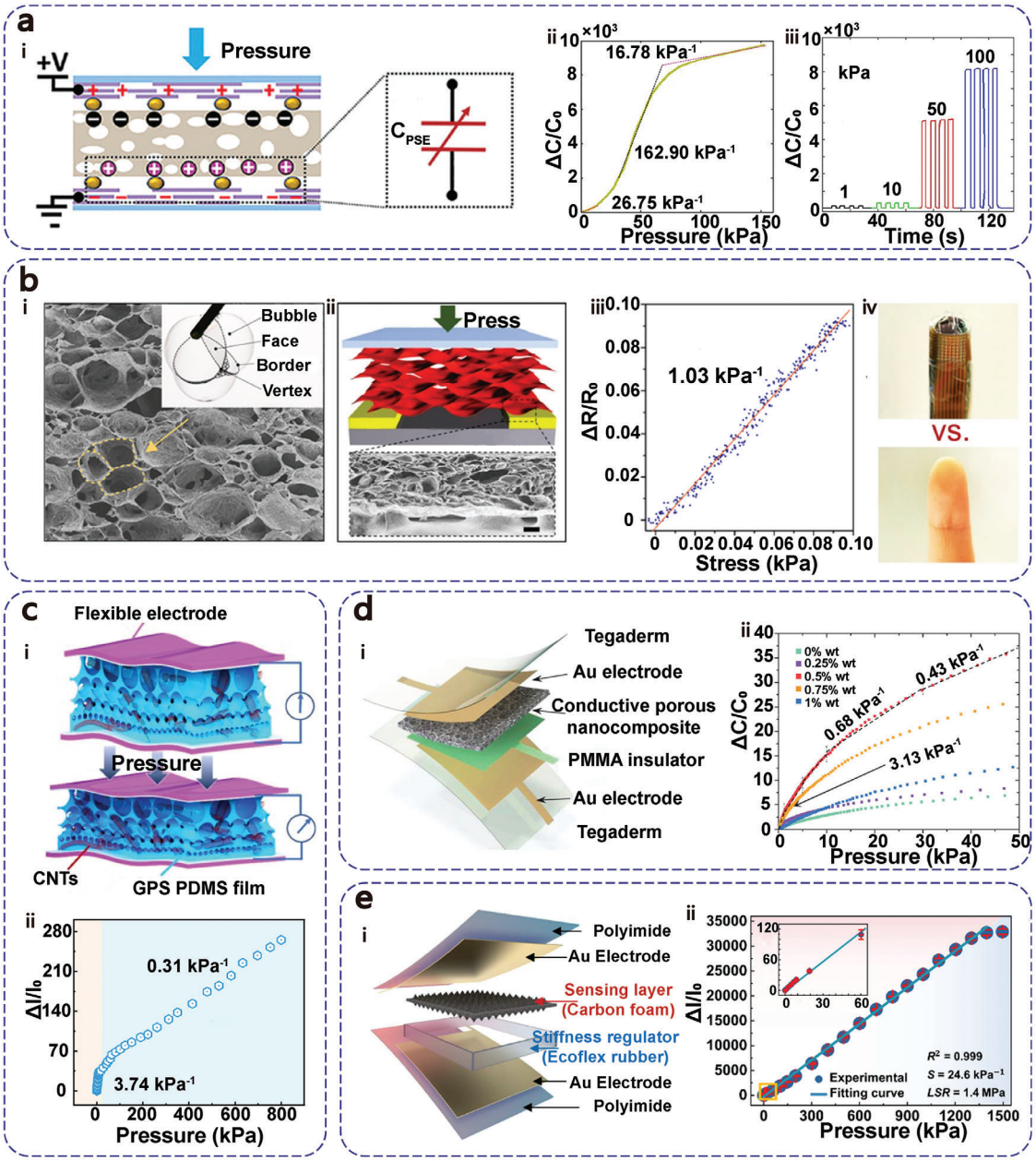

Figure 5. Sensors with microporous structures. a) i: Schematic illustration of the sensor. ii: Capacitance variation graph under pressure. iii: Capacitance variation under certain pressures. Reproduced with permission.[197] Copyright 2022, Wiley-VCH. b) i: SEM images of dried graphene aerogel. ii: Structure and SEM image of the device. iii: Resistance variation graph under pressure. iv: Images showing the graphene aerogel sensor on a robot finger versus a human finger. Reproduced with permission.[198] Copyright 2020, AAAS. c) i: Schematic illustration of gradient pore structure sensor. ii: Relationship between current and pressure. Reproduced with permission.[33] Copyright 2022, Elsevier. d) i: Schematic illustration of the device. ii: Capacitance change under pressure with various CNT ratios. Reproduced with permission.[199] Copyright 2021, Wiley-VCH. e) i: Exploded view illustrating the design layout. ii: Current change under pressure. Reproduced with permission.[201] Copyright 2023, Springer Nature.

method. The sensor had a sensitivity of 35 kPa^{-1}. Guo and co-workers[197] developed a flowable ionic electronic tactile sensor by using highly conductive PEDOT:PSS film decorated PMMA microspheres as pseudocapacitive electrodes, and using solution casting and freeze-drying, compounding porous polyurethane foam with Na+/Cl ion-rich PVA hydrogel as a polymer electrolyte (**Figure** 5a). Taking advantage of the high false capacitance and well-designed microstructure, the tactile sensor had been developed with a sensitivity of 162.90 kPa^{-1}, detection range of 160 kPa, detection limit of 30 Pa, response time of 25 ms, and excellent repeatability and durability. Gao and co-workers[198] invented the method of hydroplastic foaming (HPF), which converted layered graphene oxide (GO) solids into graphene aerogel by injecting a blowing agent (Figure 5b). This method could be used for continuous mass production of graphene aerogel. By exploring bubble formation patterns, precise control of the

cell wall thickness of 8–40 nm and density of 5–20 mg cm^{-3} of the film was achieved. Stable bubble agglomeration resulted in a seamless substrate connection of 2D lamellae, resulting in superior mechanical stability of the gel capsule with a sensitivity of 1.03 Kpa^{-1} and a detection limit of 4 mN. Hu and co-workers[33] prepared PDMS/CNT gradient pore microstructure films by autoclave foaming, and fabricated piezoresistive flexible sensors using ITO/PET films as electrodes (Figure 5c). This film had a gradient modulus of elasticity along the thickness of the film, similar to the dermal layer of the skin. Due to the high structural compressibility and stress adaptability of the porous film, the tactile sensor could achieve a sensitivity of 3.74 kPa^{-1} with a high-pressure resolution of 0.06%, a response range of 800 kPa, a fast response time of 15 ms, a low detection limit of 1.65 Pa and great cycling stability. Lu and co-workers[199] first developed a tactile sensor with a hybrid response of mixing piezoresistive and piezocapacitive effects using sponge Ni as a template to invert a conductive porous nanocomposite based on Ecoflex/CNT combined with an ultrathin insulating layer (Figure 5d). The hybrid response of piezoresistive and piezocapacitor enabled flexible pressure sensors with high resolution and a wide operating range, with 86% porosity and conductivity, with a sensitivity of 3.13 kPa^{-1} and a response range of 125 kPa. The weight of the fruit fly and the pressure generated by the human foot can both be sensitively sensed. Zhang and co-workers[200] assembled GO onto a hydrophilic PU sponge, then underwent in situ reduction, and wrapped a conductive polyaniline nanohair (PANIH) array on an RGO sheet to assemble a piezoresistive flexible sensor. The sensor could detect strain deformation of 25 kPa and had a response/recovery time of 22 ms/20 ms, ultrasensitive load sensing of feathers of 25 mg, and static tremor at 5 Hz.

Most of the microporous sensors' Young's modulus is small, thus apt to reach saturation of high sensitivity linear range limit at the order of 100 Kpa. In order to develop sensors with both high sensitivity and high linearity, Zhou and co-workers[201] integrated the advantages of micropyramid and microporous structure, using a dual-sided pyramidal foam carbon array as the sensing layer with high nonlinear piezoresistivity (Figure 5e). On the other hand, the relationship between compressive strain and pressure was also nonlinear. In order to broaden the pressure sensing range, an elastic spacer was introduced around the sensing layer as a stiffness regulator to adjust the load share on the sensing layer, so that the attenuation constant of the resistivity matched the stiffness constant, and the combined effect of the nonlinearity of the elasticity of the stiffness regulator and the piezoresistivity of the active layer resulted in the high linearity with a sensitivity of up to 24.6 kPa^{-1} and excellent linearity ($R^2 > 0.99$) ranging from 0 to 1.4 MPa.

3.5. Topological Interconnect Microstructures

In flexible tactile sensors with micropyramids, microhemispheres, and micropillars, the functional layers are often arranged in a stacked manner without the need for interlayer bonding. In general, layers typically consist of diverse materials, which is prone to cause significant mechanical mismatch. When the sensor is exposed to large deformations like high pressure or shear forces, devices may easily detach or delaminate, causing interface failure. In order to prevent device failure under large deformations, topological interconnects are used to connect their functional layers to each other, resulting in a new network that penetrates the adhesion network to form a tough and robust interface.

Guo and co-workers[35] fabricated piezocapacitive tactile sensors with high interfacial stability and avoided the mechanical mismatch between layers through a quasi-homogeneous composition composed of PDMS/CNTs (**Figure 6a**). The capacitive sensor consisted of micro-cone electrodes with 7 wt.% CNTs, dielectric layers with 2 wt.% CNTs, and planar electrode layers with 7 wt.% CNTs, and the strong topology between the different functional layers enabled it a high interfacial toughness of 390 J m^{-2}, an ultrafast response time of 6 ms, a wide detection range of 400 Kpa, and a sensitivity of 0.15 kPa^{-1}. Compared with ordinary commercial devices, the high interface toughness ensured its good robustness, high stability, and high-fidelity sensing signals under harsh mechanical conditions. Lu and co-workers[202] designed a flexible piezocapacitive tactile sensor based on topology interconnected micropillar arrays (Figure 6b). The PDMS dielectric layer structure was prepared by photoresist inversion with an inclined micropillar array, which was highly uniform across a significant surface and was firmly adhered to the Au-coated electrode. Inclined micropillar arrays exhibited bending rather than compression deformation when force was applied, making it easier to reduce the distance between the two electrodes. Notably, the sensor eliminated the presence of an uncertain air gap between the dielectric layer and the electrode, and the strong bond and robust construction of the sensor gave the sensor high stability and reliable capacitive response, resulting in a pressure sensitivity of 0.42 kPa^{-1} and a small detection limit of 1 Pa. Zhou and co-workers[203] obtained a piezocapacitive sensor with an ultrawide detection range of 800 Kpa, a sensitivity of 0.0124 kPa^{-1}, and a detection limit of 2 Pa using a magnetic field-assisted in situ formation of a spine array as the dielectric layer of a capacitive sensor (Figure 6c). This method did not require the assistance of a template, and the preparation process was simple. The sensor's topological interconnect design enabled dependable and reversible shear detection, offering a sensitivity of 0.0752 N^{-1}.

3.6. Microcrack Structures

Conventional microcrack structures are often applied in strain sensors, typically made by ultrathin metal films. Microcracks are pulled apart when the sensor is stretched, and the tunnel effect is sharply reduced, resulting in a sharp increase in resistance and ultrahigh sensitivity. Wang and co-workers[204] fabricated an ultrasensitive strain sensor using Au/Ti thin film on the PDMS substrate. The sensor had a high GF of 5000 under 1% strain with the capability of detecting pulse waves, joint bending, vocal vibration, and other biologically associated skin deformation. Pan and co-workers[205] demonstrated an Au/PDMS-based ultrathin strain sensor with GF of 44013 under 0.88% strain which was capable of tiny deformation. However, microcrack formation tends to be random in strain sensors, which limits the uniformity, repeatability, and mechanical robustness of the device's performance. Utilizing the high sensitivity of the microcrack structure, the researchers developed the controllable formation of

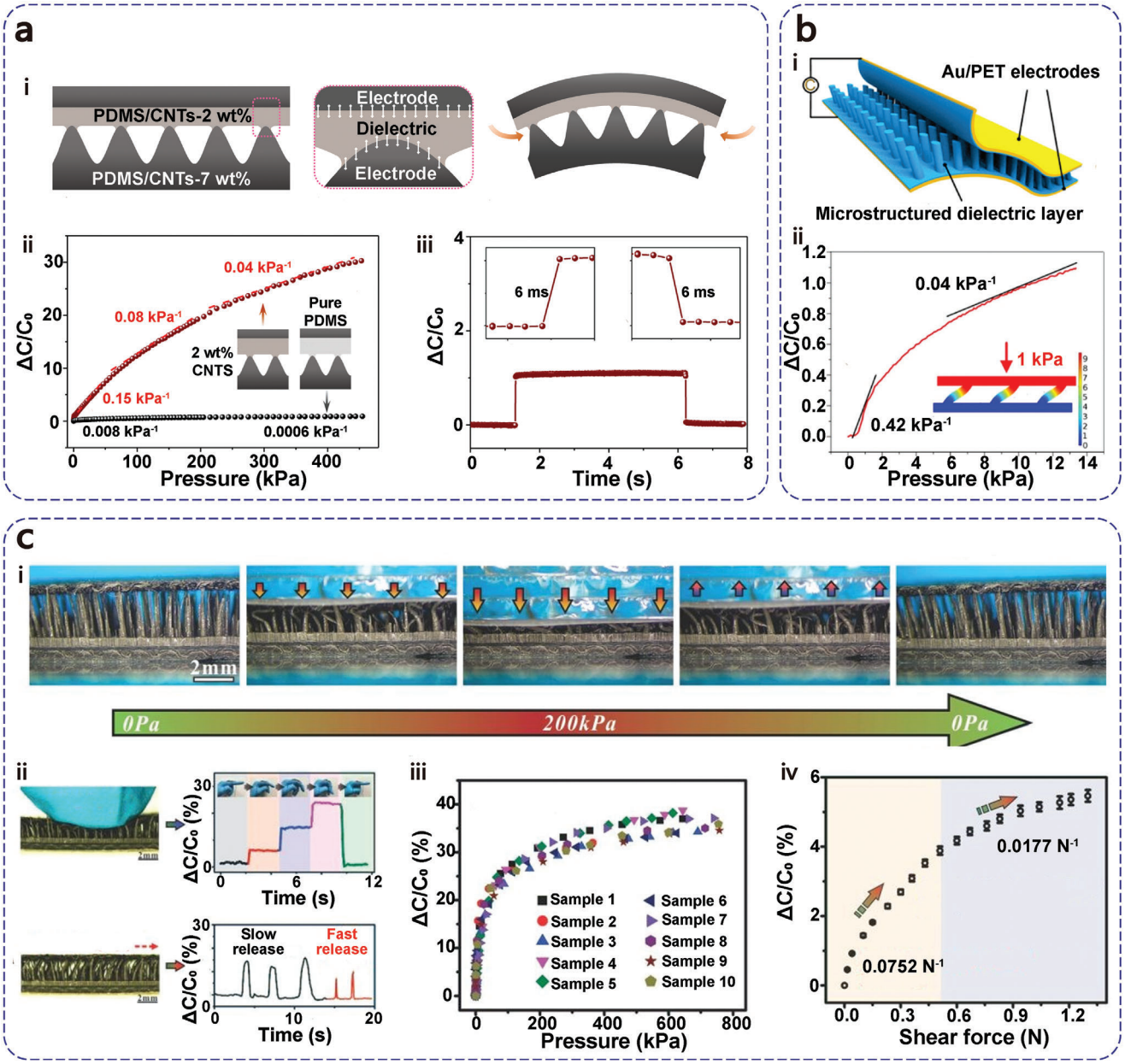

Figure 6. Sensors with topological interconnect microstructures. a) i: Schematic illustration of the Topological interconnect layers. ii: Capacitance changes under pressure. iii: Response and relaxation time. Reproduced with permission.[35] Copyright 2022, Springer Nature. b) i: Schematic illustration of the device. ii: Pressure-response curves. Reproduced with permission.[202] Copyright 2019, American Chemical Society. c) i: Cross-sectional images of microstructure deformations under pressure. ii: Real-time reactions to finger pressure and shear force. iii: Capacitance change under pressure with various samples. iv: Capacitance variation to shear force. Reproduced with permission.[203] Copyright 2020, The Royal Society of Chemistry.

microcracks and applied them to the vibration detection and pressure detection of tactile sensors.

By utilizing a solvent-induced swelling technique to create a template for generating orderly arrays of microcracks on the inner surface (**Figure** 7a). The piezoresistive performance of the device was from the change of contact area between the interlocking electrode patterns of the microcrack arrays on PDMS film. The device exhibited good performance with a sensitivity of 27.79 kPa^{-1}, a short response/recovery time of 111/95 ms, a low detectable pressure limit, and excellent repeatability.[206] Choi and co-workers[34] showed an ultrasensitive resistive sensor by hole-induced controllable microcrack formation (Figure 7b). The device featured structured holes on its surface that focused stress around these areas, leading to the formation of consistent cracks linking the holes throughout the surface. The controlled formation of linear cracks led to an exponential dependence of drag strain with a high sensitivity of 606.15 kPa^{-1} at low pressure and more than 1×10^5 kPa^{-1} in the pressure range of 8–9.5 kPa, high durability, and repeatability. Tee and co-workers[207] fabricated piezoresistive microcrack sensors by fabricating

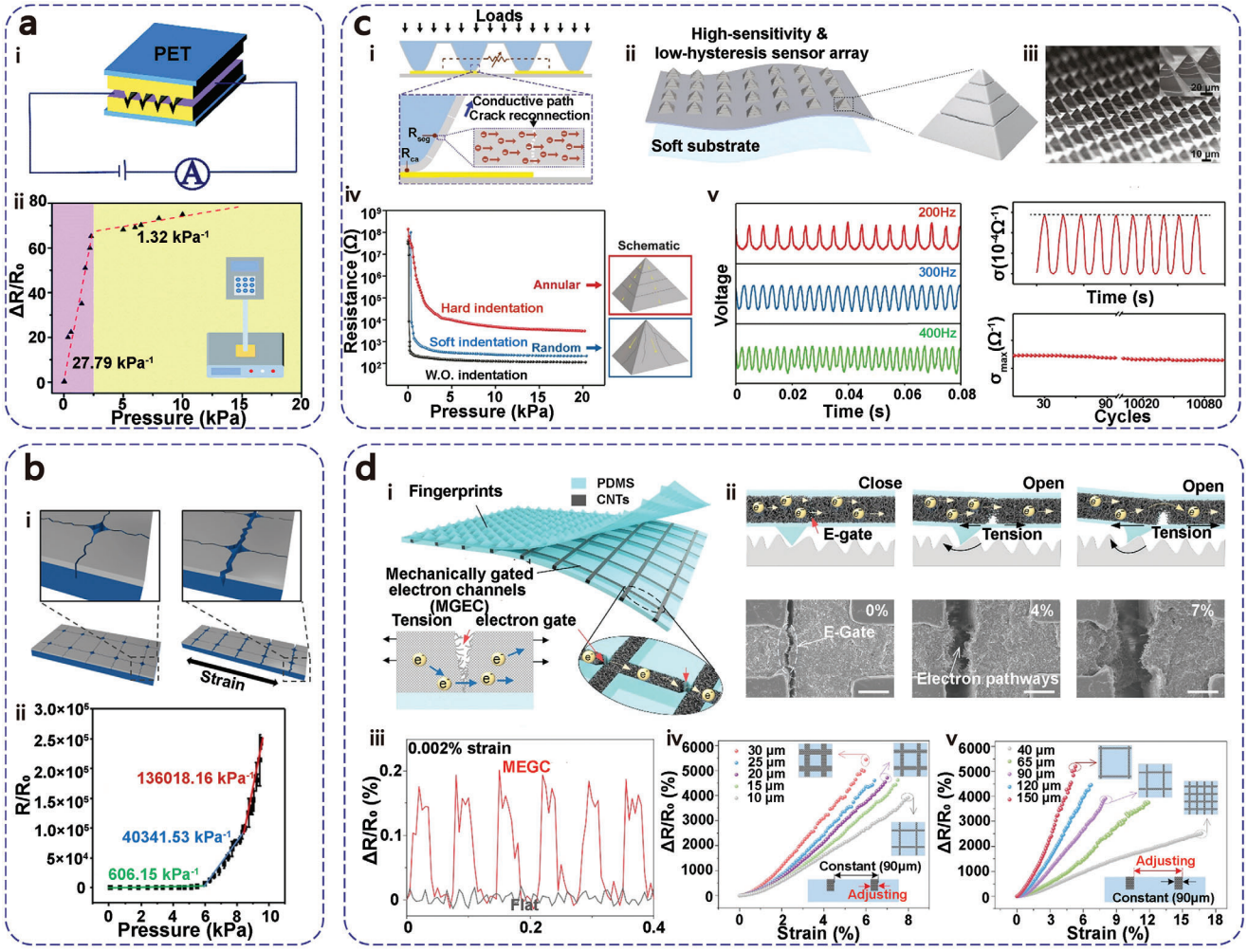

Figure 7. Sensors with microcrack structures. a) i: Schematic illustration of the device. ii: Sensitivity of the device under pressure. Reproduced with permission.[206] Copyright 2019, The Royal Society of Chemistry. b) i: Illustrations of the sensor before and after stretching. ii: The normalized resistance data with pressure. Reproduced with permission.[34] Copyright 2017, Springer Nature. c) i: Diagram of the periodically fractured micropyramids. ii: SEM image of Pt-coated micropyramid arrays. iii: The optimized electromechanical property of the device. iv: The output voltage of the device under different frequencies. v: Cyclic testing of the device. Reproduced with permission.[207] Copyright 2020, National Academy of Sciences. d) i: Schematic illustration of the device. ii: Sliding sensing process of the device. iii: Detection ability of extremely subtle strain. iv, v: Performance contrast of devices with various channel widths and channel periods. Reproduced with permission.[208] Copyright 2022, Elsevier.

controllable annular microcracks on thin platinum Pt films applied onto the micropyramids of PDMS to balance between sensitivity and hysteresis in tactile sensors when employing soft materials (Figure 7c). Piezoresistive sensors using 3D metal annular crack arrays on polymer microstructures had a high sensitivity of 107 Ω kPa^{-1}, low hysteresis of 2.99%, and fast response of 400 Hz over a wide pressure range of 20 kPa, far better than those made by random microcracks and microcrack-free structures. Shao and co-workers[208] fabricated a piezoresistive tactile sensor with the ability to detect vibration and surface roughness by triggering the opening and closing of V-shaped microcracks in the embedded mesh electronic channel through a pyramid-shaped artificial fingerprint (Figure 7d). By exploring the parameters of the conductive network, weakening the strain at other locations, and suppressing random cracks, ultrasensitive and fast-response sliding tactile perception was realized with good stability. The sensor had good vibration detection capability to directly recognize ultrafine surface microstructures of 5 μm at a response frequency of 485 Hz and realizes human-like roughness perception by performing Fourier transform of the collected signals to distinguish the texture of complex shapes and provide real-time feedback for grasping.

3.7. Multilevel Microstructures

In flexible tactile sensors with micropyramids, microhemispheres, and micropillars, although the microstructure surface produces more deformation than the planar surface under the same external force, bringing higher sensitivity, the uniform geometric microstructure hinders their further deformation. The linearity of the device is often not high, usually less than 2 kPa,

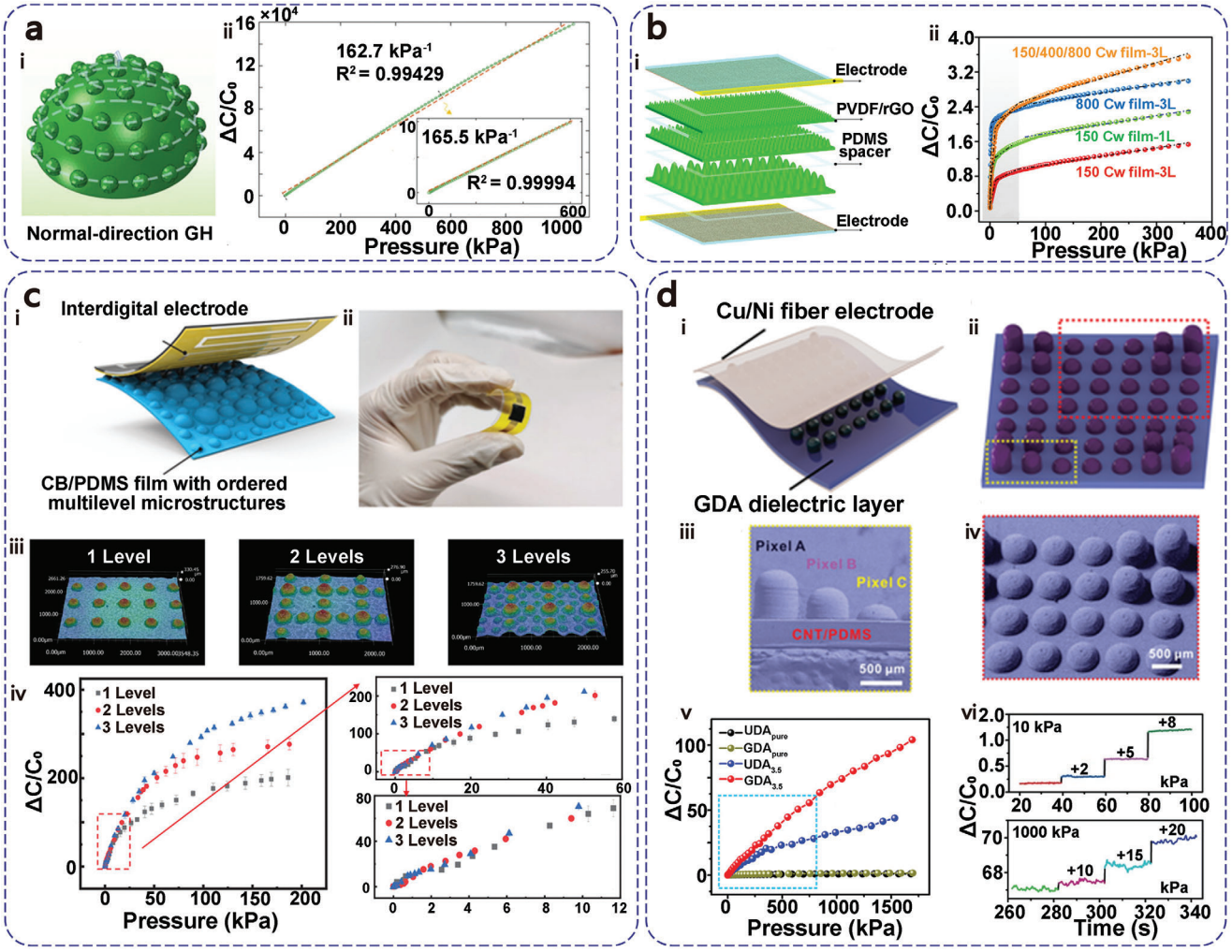

Figure 8. Sensors with multilevel Microstructures. a) i: Schematic diagram of the graded hemispherical structures. ii: The response curve of the sensor. Reproduced with permission.[215] Copyright 2023, American Chemical Society. b) i: Exploded diagram of the device. ii: Capacitance variation with different stacked layers. Reproduced with permission.[212] Copyright 2022, Wiley-VCH. c) i: Schematic diagram of the sensor. ii: Optical image of the device. iii: Contact areas with 1, 2, and 3 levels. iv: Current changes of different microstructure levels under different pressures. Reproduced with permission.[36] Copyright 2022, Wiley-VCH. d) i, ii: Diagram of the device and the active layer. iii, iv: SEM images of the active layer. v: Capacitance variation under pressure. vi: Tiny pressure detect capability under high pressure. Reproduced with permission.[213] Copyright 2021, Wiley-VCH.

which limits the application scenarios of the sensor. Multilevel structures have corresponding microstructure dimensions for each stress interval to provide deformation and more contact area so that the linear range and corresponding range of the homogeneous sensor can be extended.

Most of the multilevel microstructures are on the active layers of the sensors. Sun and co-workers[209] developed piezocapacitive sensors with high linearity ($R^2 = 0.99$) within a range of 200 kPa using a multilevel microhemispherical MWCNT/PDMS dielectric layer and copper electrodes fabricated through a reverse mold. The sensor exhibited a sensitivity of 1.3 kPa^{-1}, fast response/release times of 12.5/37.5 ms, detection limit of 35 Pa, and high repeatability of 10 000 cycles. Shen and co-workers[210] showed piezocapacitive tactile sensors incorporating a 3D multilevel structure known as the P(VDF-TrFE) fiber-TiO_2 pillar-TiO_2 thorn structure with a high sensitivity of 0.163 kPa^{-1}, wide pressure sensing range of 200 kPa and fast response/relaxation time of 5.6 ms. Sun and co-workers[211] reported a piezoresistive tactile sensor based on an interdigital-shaped multilevel microstructure. The multilevel structure consisted of three layers of CNT/PDMS films with different modulus, conductivity, and microstructure gradients. The sensor had a high sensitivity of 153.3 kPa^{-1}, a low detection limit of 0.5 Pa, and an ultrawide detection range of 1.3 MPa. Wang and co-workers[212] fabricated a flexible capacitive pressure sensor utilizing a three-layer hierarchical microstructured PVDF/rGO thin film with irregular protrusions of 150 Cw, 400 Cw, and 800 Cw, respectively (**Figure 8b**). Because of the combined impact of the compressibility of the layered multilayer film under pressure and the efficient distribution of stress, the sensor had a good sensitivity of 0.18 kPa^{-1} over a wide linear range to 11 kPa and was not saturated at a high-pressure range of 360 kPa. In addition, the sensor exhibited excellent stability over ten cycles at a pressure of 3000 kPa and successfully responded to the pressure of 0.16 g of fallen leaves

and 100 g of weight as well as pressure from high heels. These remarkable characteristics were credited to the compressibility of the stratified arrangement and the efficient stress distribution among the stacked layers. Zhou and co-workers[36] designed a flexible resistive pressure sensor with an orderly three-stage micro-hemispherical structure. The sensor is prepared by molding PDMS in the glass plate template made by laser marking technology, and spraying carbon black on the PDMS film (Figure 8c). The sensor had a sensitivity of 8.3 kPa^{-1} at low pressure and a sensitivity of 1.5 kPa^{-1} at high pressure, which was 250% higher than that of single-level microstructured flexible sensors. The sensor can detect slight signal change at relatively high pressures with a detection limit of 10 Pa, a response time of less than 70 ms, and excellent durability of more than 10 000 cycles. Zhou and co-workers[213] obtained a capacitive sensor based on a dielectric layer with a high-k CNT/PDMS multilevel microhemispherical structure by designing a plastic template with micro-engraving technology and inverted the mold with a CNT/PDMS mixture (Figure 8d). The gradient micro-hemispherical pixels could be made to contact the electrode in turn from high to low with the increase of stress by matching the number and height of gradient micro-hemispherical pixels, so as to achieve a wide linear range. The sensor maintained a high sensitivity of 0.065 kPa^{-1} over an ultrawide linear range of up to 1700 kPa. Yang and co-workers[214] prepared a multilevel structure composed of a flexible, tentacle-shaped microcone on the upper level, a porous microdome in the middle, and a cylindrical micropillar at the base through laser engraving acrylic sheets and molding with MWCNTs/PDMS composite materials. The slender shape of the microcone, the porous microdome, and the cylindrical microcartridge provided high-performance sensing capabilities at low pressure (<10 Pa), medium pressure, and high pressure (>1 kPa), respectively. This innovative microstructure enabled the newly designed piezoresistive sensor to have a higher sensitivity of 35.51 kPa^{-1}, a wider pressure sensing range of up to 23 kPa, and a detection limit as low as 2 Pa than other reported electromechanical sensors.

For sensors with microstructures on the electrodes, Wang and co-workers[215] fabricated piezocapacitive tactile sensors composed of flexible multilevel microhemisphere structure array electrodes made of PDMS/CNTs/Au, and dielectric layer consisting of PVDF-co-HFP and (EMIM[TFSI]) ionic gel dielectric layer (Figure 8a). The sensor exhibited record-high linearity ($R^2 = 0.99994$) up to 600 kPa ultrahigh linearity ($R^2 = 0.994$) and a high sensitivity of 162.7 kPa^{-1} up to 1 MPa with a detection limit of 18 Pa, a response relaxation time of 28 ms, and excellent consistency under repeated testing.

3.8. Random Rough Surface

Using random rough surfaces is another good choice to cope with the need for high sensitivity and wide response range besides using multilevel structures. Due to the limitations of template design and processing technology, the size of micropyramids, micropillars, and micro-hemispherical arrays are in the order of 100 microns, while the microstructure size of random rough surface can be achieved from a few microns to more than ten microns, which is not easy to suffer mechanical failure and thus increases the long-term stability of the sensor. At the same time, random rough surfaces have a more significant change in capacitive surface area when compressed, and therefore, tend to have higher sensitivity and a wider response range.

Guo and co-workers[37] poured PVA/H_3PO_4 ionic gels on a specific sandpaper to obtain random rough structures composed of unstable protrusion microstructures at different heights (**Figure 9a**). These protrusions were easily folded or bent when compressed. These protrusions also had complementary grooves that could nest within each other, producing additional compressibility under pressure. The resulting rough surface also created a sufficient contact area with the electrode, resulting in a notable sensitivity of 3300 kPa^{-1} and fine pressure resolution ≈10 Pa across a broad pressure span of up to 360 kPa. The sensor also showed excellent mechanical stability with no significant fatigue. Due to the large specific capacitance of the ion electronic interface, the sensor had a good signal-to-noise ratio. Cai and co-workers[216] fabricated capacitive tactile sensors with random rough structures by using the inverted PDMS dielectric layer of the eggshell inner membrane and composite electrodes based on 2D MXene sheets and 1D Ag NWs (Figure 9b). The fibrous eggshell inner membrane acted as a nanoscale template, providing a fine microstructure that contributed to the significant deformation of the PDMS dielectric layer in response to external stimuli. As a result, microstructured sensors offered higher sensitivity, a wide detection range of 600 kPa, a lower detection limit of 16 mg, a fast response time, long-term stability, and repeatability, especially in the high-pressure range. Gao and co-workers[217] obtained high-performance piezoresistive tactile sensors by pouring PU on the surface of sandpapers to obtain PU layers with randomly rough surfaces (Figure 9c). The sprayed MXene on the random rough surface of PU and PI substrates acted as a sensitive layer and interdigital electrodes, respectively. The sensor had a high sensitivity of 509.8 kPa^{-1}, a detection range of 20 kPa, and response and recovery speed of 67.3 and 44.8 ms with good robustness. The hydrogen bonding of the PU enabled the device a self-healing capability with little effect on sensitivity after the self-healing of active layer fractures.

3.9. Animal Biomimetic Microstructures

Serves as the primary tactile sensory organ in animals, capable of detecting external stimuli like pressure, strain, temperature, and moisture. Skin tissue is rich in microstructured tissues, which can be used as a source of inspiration for biomimetics in the microstructure design of tactile sensors. Interlocking microstructures between the epidermis and dermis, such as spinosum structures, and wrinkle-like microstructures on the skin surface, such as fingerprint structures, play a key role in sensitizing and reacting when the skin is weakly stimulated, generating local and high-stress concentrations at the tips of interlocking and wrinkle structures, enhancing stress perception. Therefore, the inclusion of skin-inspired microstructures in the design of tactile sensors can undergo greater shape changes and conductive network changes under pressure loading, therefore effectively improving the change of sensing material-electrode contact area and the sensing performance, especially the response to microstimuli.

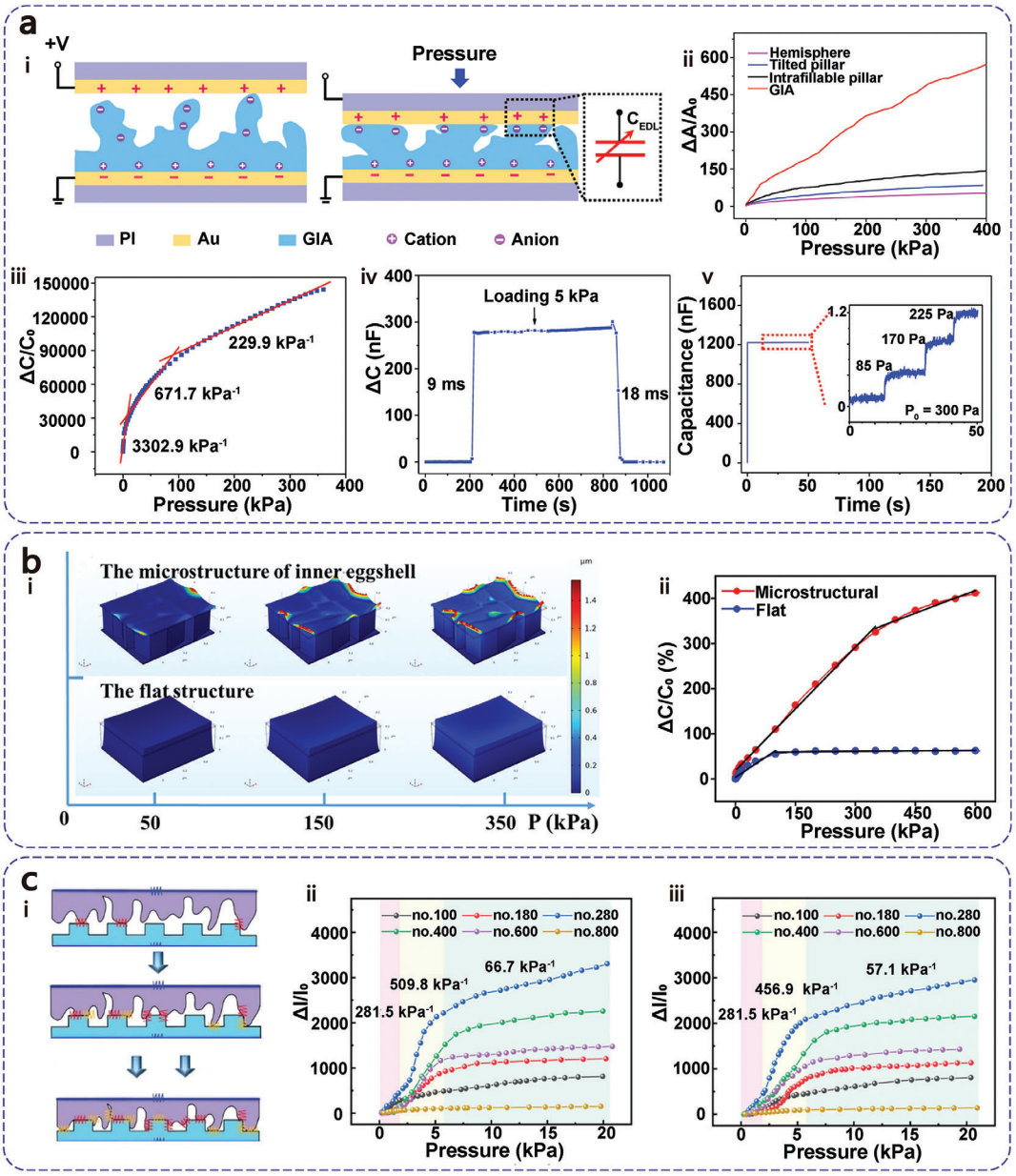

Figure 9. Sensors with randomly rough surfaces. a) i: Schematic diagram of the device with and without pressure. ii: Contact area variation with various structures. iii: Change of capacitance over the pressure. iv: Response time of the device. v: Slight pressure capability under 300 kPa. Reproduced with permission.[37] Copyright 2020, Springer Nature. b) i: Schematic diagram of the flat and microstructured sensors under the external pressure from Comsol simulation. ii: Sensitivity comparison of the flat and microstructured sensors. Reproduced with permission.[216] Copyright 2021, Springer Nature. c) i: Diagrams of the device in different pressure levels. ii: Sensitivity of the sensor molded from abrasive papers with various roughness. iii: Sensitivities of the sensors after self-healing. Reproduced with permission.[217] Copyright 2022, Wiley-VCH.

Shen and co-workers[218] used Ti_3C_2 Mxene and natural microcapsules with interlocking structures to fabricate piezoresistive tactile sensors with skin receptor structure, which could achieve high deformation under various external stimuli (**Figure 10a**). The flexible sensor with a skin-like interlocking structure had a pressure sensitivity of 24.63 kPa^{-1}, which was tenfold higher than the planar flexible sensor, with a low elastic modulus of 0.73 MPa, a fast response time of 14 ms, good cycle reproducibility and stability of 5000 cycles. Bao and co-workers[38] simulated hills and mechanoreceptors in spinosum structures by constructing arrayed CNT electrodes on the surface of a PU microhemisphere and a micropyramid array respectively (Figure 10b). The sensor could detect the magnitude and direction of normal and shear forces at the same time. The sensor had a pressure sensitivity of 0.19 kPa^{-1} and a shear sensitivity of 3.0 kPa^{-1}. For several consecutive pressure runs from 0 to 1800 kPa, the sensor output was highly stable and repeatable. Zhang and co-workers[219] fabricated a piezoresistive flexible

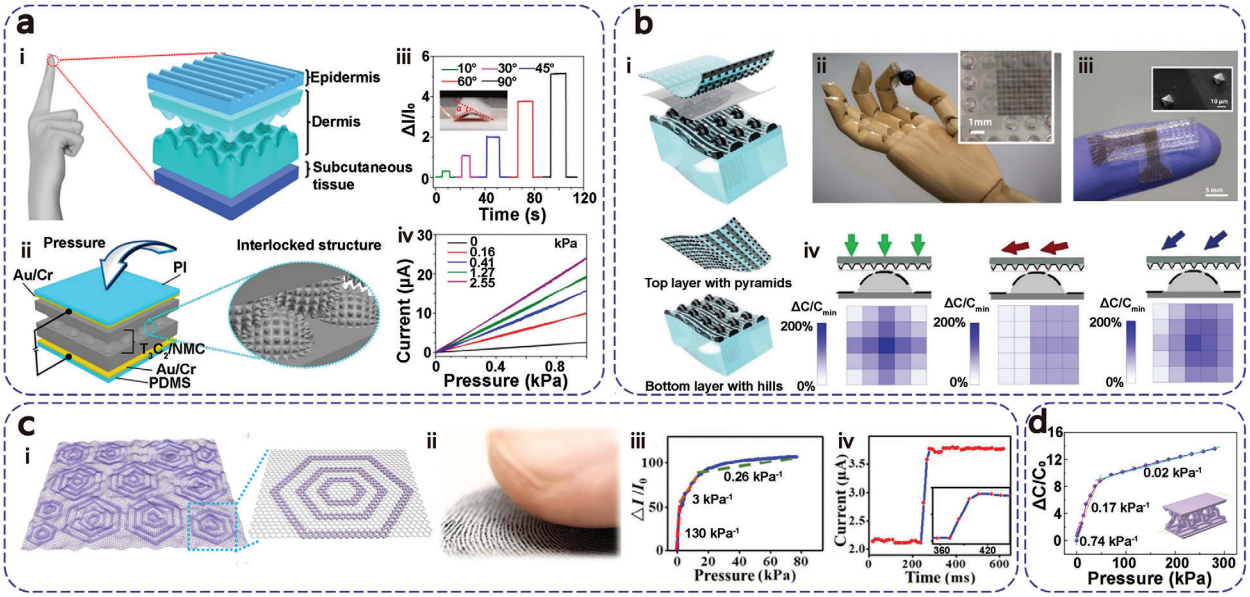

Figure 10. Sensors with animal biomimetic microstructures. a) i: Characteristic human skin microstructures. ii: Schematic diagram of the device. iii: Pressure response under various bending levels. iv: Current under various pressures. Reproduced with permission.[218] Copyright 2019, American Chemical Society. b) i: Diagram illustrating the soft biomimetic sensor. ii, iii: Images and SEM images showing the pyramids and electrodes interconnects of the sensor. iv: Cross-sectional perspective under different stress directions. Reproduced with permission.[38] Copyright 2018, AAAS. c) i, ii: Illustration of the 3D graphene in comparison with a human fingerprint. iii: Current–pressure plot for pressure. iv: Response time of the device. Reproduced with permission.[219] Copyright 2018, Springer Nature. d) Schematic diagram of the device and its capacitance response curve. Reproduced with permission.[221] Copyright 2023, American Chemical Society.

pressure sensor that mimicked the morphology of fingerprint epidermal ridges by using a unique self-assembled concentric nanoribbon loop structure on graphene thin films during chemical vapor deposition and growth (Figure 10c). The sensor had a high sensitivity of 110 kPa^{-1}, a high sensing range of up to 75 kPa, a low detection limit of 0.2 Pa, a high response speed of less than 30 kPa, and good stability over 10 000 load/unload cycles. Lu and co-workers[220] developed skin-inspired flexible tactile sensors incorporating interfacial microstructures on cellulose fiber substrates. The device mimiked the epidermis and dermis with the cellulose fiber substrate and used screen printing conductive ink to construct the surface microstructure to imitate the spinosum structure. The microstructure brought higher stress concentration at the tip and significant electrical contact changes when applying pressure. The sensor had a sensitivity of 14.4 kPa^{-1} and a fast recovery time of 2.5 ms. Zhao and co-workers[221] fabricated piezocapacitive tactile sensor based on the microstructure of cheetah legs (Figure 10d). The microstructured PDMS dielectric layer was molded by 3D-printed PLA templates and the electrodes were made by conductive silver glue. The sensor exhibited a sensitivity of 0.75 kPa^{-1}, a sensing range of 280 kPa, and durability of 24 000 cycles.

3.10. Plant Biomimetic Microstructures

Most microstructures involve a mold transfer process during preparation, often complex and time-consuming. Sensors fabricated using natural templates can achieve comparable performance levels without the need for costly and intricate equipment and procedures and have been extensively studied due to their eco-friendliness, abundance, renewability, sustainability, biodegradability, and cost-effectiveness compared with the template obtained by micromachining methods. The surfaces of leaves or petals feature textured microstructures, and employing them as templates can greatly enhance sensitivity. In addition, it is also possible to expand the theoretical boundaries of existing sensor sensitivity and develop sensors with new mechanisms by imitating the special microstructure of plant surfaces.

The microstructure of lotus leaves is a widely applied biomimetic structure in tactile sensors because the lotus leaf surface is uniformly covered with micro-protrusions of ≈10 μm in diameter and depth. These structures can be easily replicated on thin films such as PDMS using the secondary templating method. They can be used as electrode layers and active layers in sensors, thereby enhancing the performance of the sensors. Zhang and co-workers[222] fabricated capacitive flexible tactile sensors by utilizing the surface of natural lotus leaves as a template to replicate PDMS with deposited gold on the surface as electrodes and polystyrene microspheres as the dielectric layer. The sensors exhibited a sensitivity of 0.815 kPa^{-1}, a wide dynamic response range of 500 kPa, and a response time of 38 ms. These performance characteristics were superior to sensors without lotus leaf microstructures. Fang and co-workers[223] fabricated piezoresistive flexible tactile sensors by spray-coating graphene thin films onto PDMS substrates with the lotus leaf surface replicated using secondary templating. The lotus leaf surface imparted microstructures to the PDMS surface, resulting in a rapid and stable increase in the contact area with the load. The sensors exhibited a linear range of 25 kPa, a sensitivity of

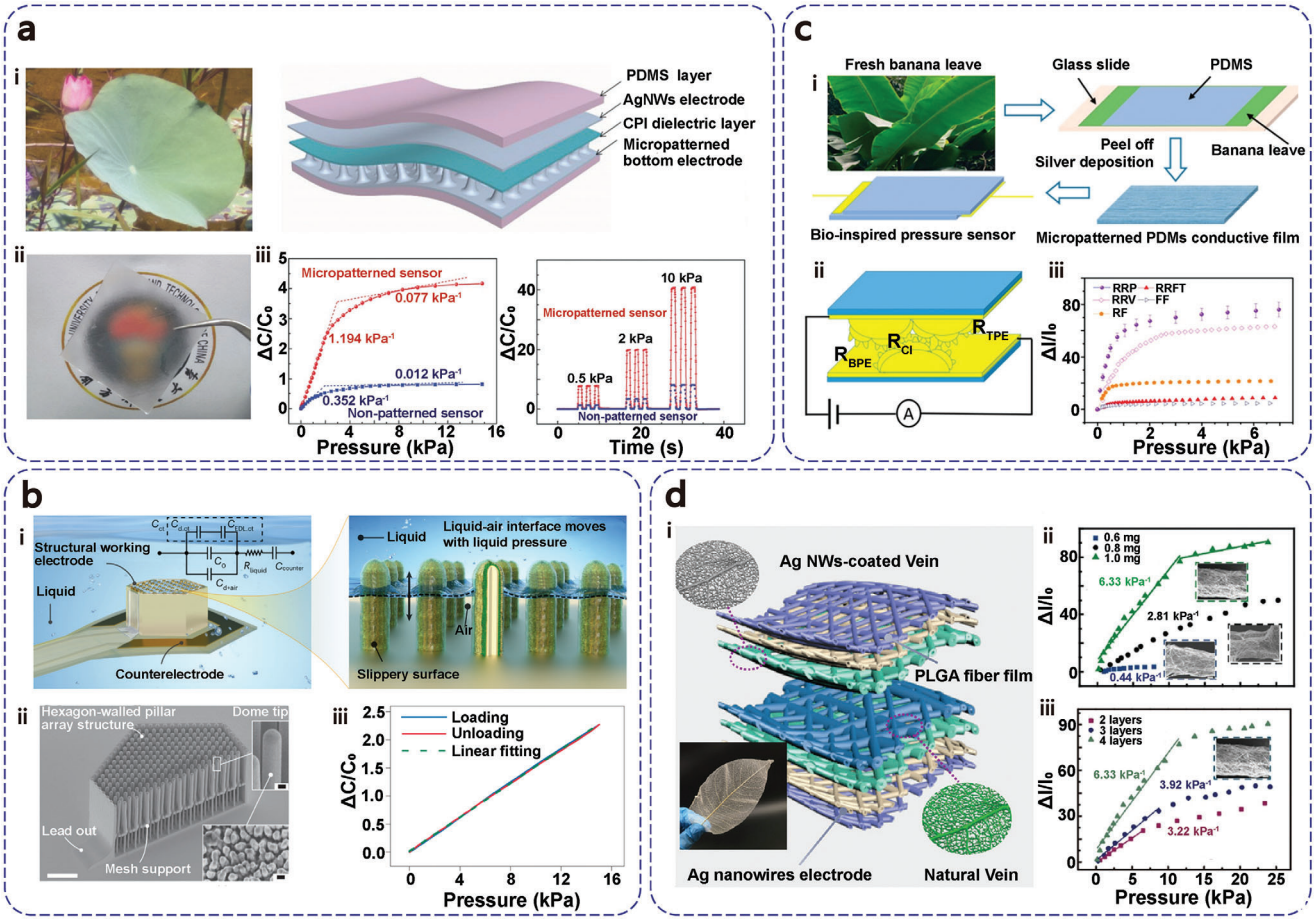

Figure 11. Sensors with Plant biomimetic microstructures. a) i: Photo of a lotus leaf and schematic illustration of the device. ii: Image of the active layer. iii: Sensitivity of the sensors with or without microstructures iv: Repeated real-time responses to the pressure for the two types of sensors. Reproduced with permission.[224] Copyright 2018, Wiley-VCH. b) i: Illustration of the sensor design. ii: SEM images of the device. iii: Pressure-sensing response of the sensor. Reproduced with permission.[39] Copyright 2023, Springer Nature. c) i: Fabrication process of the pressure sensors. ii: Schematic diagram of the sensors. iii: Current variation under pressure for different active layer types. Reproduced with permission.[227] Copyright 2017, American Chemical Society. d) i: Multilayer structure of the device. ii: Current variation under pressure for different Ag NWs concentrations. iii: Current variation under pressure for different layer levels. Reproduced with permission.[228] Copyright 2022, Wiley-VCH.

1.2 kPa^{-1}, a detection limit of 5 Pa, and a stability of 1000 cycles. Guo and co-workers[224] created highly sensitive flexible tactile sensors by combining microstructured PDMS film coated with ultrafine silver nanowires as the bottom electrode, a polyimide dielectric layer, and a silver nanowire top electrode (**Figure 11a**). The PDMS film replicated the natural lotus leaf structure, reproducing the high aspect ratio and low-density microprotrusions on the lotus leaf surface. The sensor exhibited a high sensitivity of ≈1.2 kPa^{-1}, an ultralow detection limit of 0.8 Pa, and a fast response time of 36 ms, a high robustness of 100 000 cycles without fatigue. Finite element analysis illustrated that the sparse microprotrusions with high aspect ratios played a crucial role in attaining high sensitivity, low detection thresholds, and swift responses to external stimuli.

Besides using a lotus leaf as a template, Tee and co-workers[39] mimicked the air retention phenomenon observed on the lotus leaf surface in water by designing a microcolumn array structure in a hexagonal chamber, utilizing the solid–liquid–liquid–gas multiphase interface and the trapped elastic air layer to modulate the capacitance variation on the interface with pressure (Figure 11b). This design enabled nearly frictionless movement of the gas–liquid contact line and achieved excellent linearity (R^2 = 0.99944), ultralow hysteresis of 1.34%, and high sensitivity of 79.1 pF·kPa^{-1}. The sensor demonstrated the capability for highly sensitive and accurate pressure monitoring in complex fluid environments.

In addition to the surface microstructure of lotus leaves, other types of leaf structures are also widely used as plant biomimetic microstructures in tactile sensors. Zhang and co-workers[225] fabricated a piezoresistive sensor using microstructured PDMS molded from natural leaves as a flexible matrix and directly grown CNTs/graphene (ACNT/G) by chemical vapor deposition as electrodes. flexible pressure sensor using ACNT/G was assembled by sandwiching two ACNT/G/PDMS films together with the ACNT orientations in the two films perpendicular to each other. Due to the microstructure of the ACNT/G and m-PDMS film surfaces, the sensor exhibited a high sensitivity of 19.8 kPa^{-1}, low detection limits of 0.6 Pa, fast response times of 16.7 ms, low

operating voltage of 0.03 V, and excellent stability of 350 00 cycles. Liu and co-workers[226] fabricated a pressure sensor with ultrahigh sensitivity by adsorbing 1T-MoS2 nanosheets on the surface of a porous PDMS network as the active layer and using natural leaf veins as the spacing between the active layer and the interdigitated gold electrode. The micro-network structure of the leaf vein guarantees a significant change in the contact area between the conductive layer and the electrode when pressure is applied, resulting in a wide sensing range. It has an ultrahigh sensitivity of 50.27 kPa^{-1} in the low-pressure region and 1036.04 kPa^{-1} in the high-pressure region with a linear range of 23 kPa, an ultralow detectable pressure limit of 6.2 Pa, high stability of 10 000 cycles, and a fast response time of 50 ms. Sun and co-workers[227] replicated the multilevel micro-ridge structure on the surface of banana leaves using PDMS molding and a thin silver layer was deposited on the PDMS surface as electrodes with formed microcracks on the silver layer under pressure (Figure 11c). The synergistic effect of the multilevel microstructure and microcracks resulted in a high sensitivity of 10 kPa^{-1} for pressures below 400 Pa and a sensitivity of 3.3 kPa^{-1} in the pressure range of 400–1000 Pa. The device also exhibited a low detection limit of ≈1 Pa, short response and relaxation time of 36 and 30 ms respectively, and high stability of 10 000 cycles. Pan and co-workers[228] used the natural veins of magnolia leaves coated with Ag NWs as the pressure-sensitive material, and PLGA NF film and PVA NF film as the vein encapsulation layer and electrode layer respectively to realize a tactile sensor with multilayer microstructure (Figure 11d). Because of its multilayered configuration, the pressure-sensitive layer's contact area expanded significantly under pressure, allowing the loading pressure to distribute evenly across each layer. This led to the pressure sensor demonstrating outstanding pressure-sensitive properties over a wide pressure sensing range of 11.60 kPa and a high sensitivity of 6.33 kPa^{-1}. The sensor was designed with fully biodegradable materials, which have good biodegradability and air permeability.

4. Applications

Traditional tactile sensors have found extensive applications in wearable devices and machine tactile sensations. Compared to traditional tactile sensors, flexible tactile sensors with microstructures often exhibit higher sensitivity, wider response range, and better mechanical stability, making them suitable for a broader range of applications. Flexible tactile sensors with microstructures have significantly contributed to the advancement of various intelligent systems, particularly in the fields of medical detection, sliding detection, and roughness perception, offering better application advantages. This part focuses on summarizing recent research progress in these three application areas, highlighting some representative works in these fields.

4.1. Physiological Signal Detection

Physiological signal detection is a key application field, and flexible tactile sensors with microstructures have shown enormous potential due to their superior sensitivity and detection limits, as well as their ability to detect subtle changes. These sensors can be used for various medical purposes, such as detecting heart rate, blood pressure, body temperature, and respiratory rate, thereby facilitating the use of mobile health monitoring and remote diagnosis in certain chronic diseases and rehabilitation monitoring.

Wong and co-workers[229] developed piezocapacitive tactile sensors by using a commercially available self-healing polyurethane (HPU) and silver nanowire mixture to create a micro-ridged structure as the electrode and combine HPU with graphene as the dielectric layer. The sensor exhibited high sensitivity with a value of 1.9 kPa^{-1}, a fast response time of less than 100 ms, a low detection limit of 10 Pa, and long-term durability with 1000 cycles, capable of detecting vocal cord vibrations during speech. Zhai and co-workers[230] assembled an ultrathin piezoresistive pressure sensor by stacking interdigitated Ag NFs electrodes, photopolymerized strain-limited films, and micropatterned graphene layers with a sensitivity of 30.2 kPa^{-1}. Even in the bent state, the sensor could achieve high-pressure resolution by detecting a weight of 1 g (≈150 Pa) and could measure the human pulse in different states (drinking, exercising, and resting) or analyze gripping postures. Experimental data demonstrated that the sensor array has an ultralow crosstalk effect of 33.41 dB due to its microcage structure, enabling clear pressure imaging, and can control model movements through customized programs. Liu and co-workers[231] fabricated piezocapacitive tactile sensors with interlocking asymmetric nanotips by using a commercial cone-shaped nanoporous aluminum oxide (AAO) template to mold [P(VDF-TrFE)] films. The sensor exhibited a high sensitivity of 6.58 kPa^{-1}, a low detection limit of 3 Pa, and good mechanical stability. The sensor could detect different degrees of finger joint bending, real-time pulse waveforms before and after movement, eye-opening and closing, and the motion and vibration of the trachea and esophagus, including swallowing and vocalization, with good repeatability. Moreover, the sensor is fabricated using a commercial template, opening up a new pathway for large-scale commercial production of microstructured tactile sensors. Liu and co-workers[232] designed a piezoresistive tactile sensor with an engineered microstructure on a PDMS film (**Figure 12a**). The sensor's high performance stemmed from its unique pyramid wall grid Microstructure (PWGM), where two pyramidal wall grid microstructure PDMS films stacked face-to-face formed a piezoresistive sensor with ultrahigh sensitivity over a very wide pressure range, up to 383 665.9 kPa^{-1} at a small pressure under 1.6 kPa and 1266.8 kPa^{-1} at a high pressure under 11 kPa with good robustness. can be applied to wearable devices in the healthcare field, such as detecting wrist pulse signals, and real-time current output for vocal cord vibration when speaking. Wang and co-workers[233] fabricated a piezocapacitive tactile sensor with self-assembled micro-pyramid structures by UV–ozone treatment and molding of pre-stretched PDMS films (Figure 12b). This sensor exhibited an ultrahigh sensitivity of 15.66 kPa^{-1}, an ultralow detection limit of 0.2 Pa, a fast response time of 42.4 ms, and excellent mechanical stability. It can detect various degrees of finger bending, muscle vibrations during throat swallowing and vocalization, as well as wrist pulse signals. This sensor plays a significant role in the field of wearable medical devices. Zhang and co-workers[234] designed a flexible sensor based on CNT and PDMS, which incorporates both porous and wrinkled structures in its active layer (Figure 12c). This sensor achieves simultaneous humidity sensing and pressure

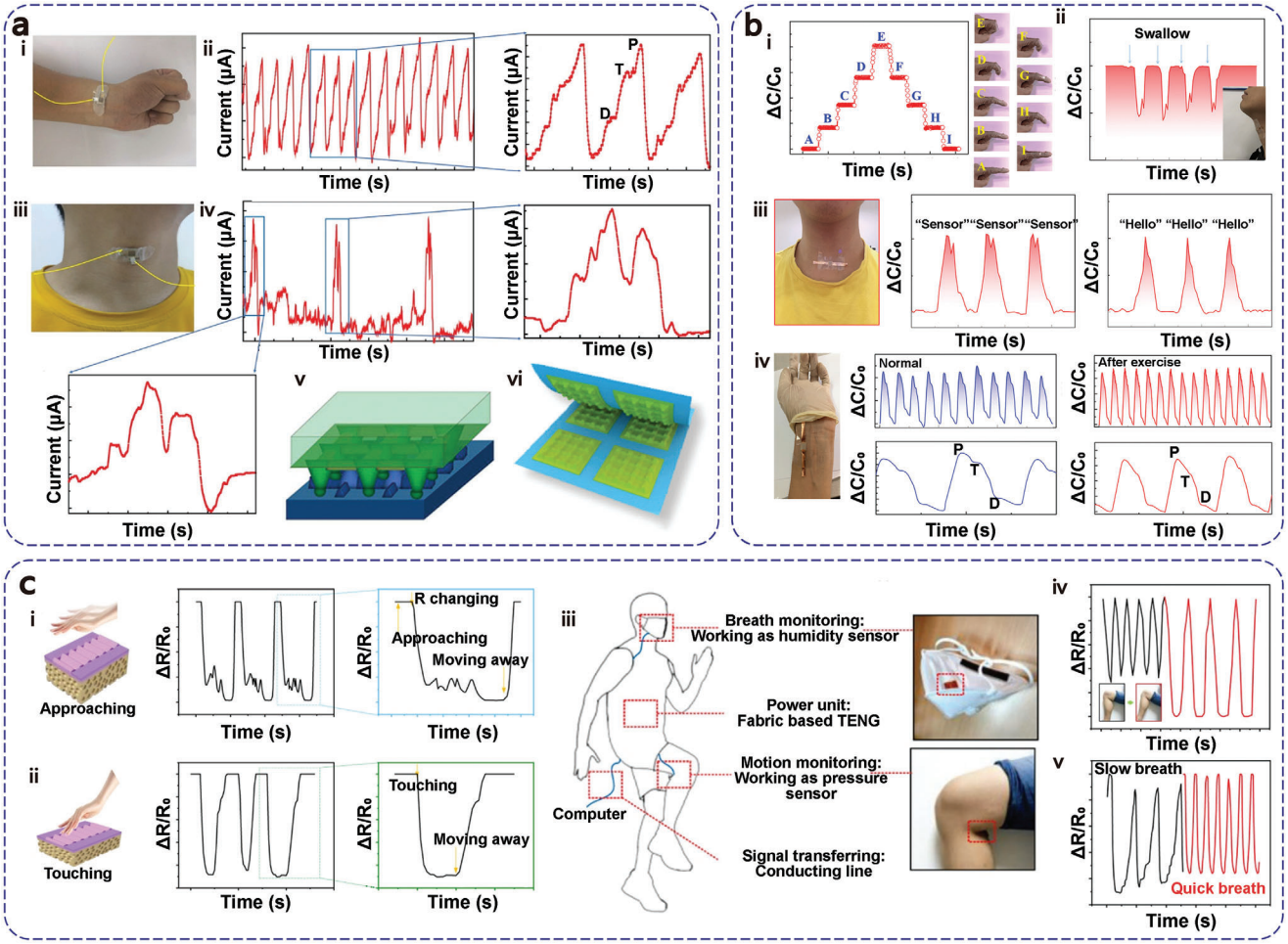

Figure 12. Sensors for Physiological signal detection. a) i, ii: Image of the device for radial artery pulse monitoring. iii, iv: Image of the device for vocal cord vibration monitoring for the pronunciation of "Good morning." v: Schematic illustration of the interlocked contact. vi: Diagram of the sensor. Reproduced with permission.[232] Copyright 2020, Wiley-VCH. b) i: Capacitance variation during finger crook. ii: Monitoring of swallowing. iii: Capacitance variation by different vocal vibrations. iv: Image of the device for radial artery pulse monitoring before and after exercise. Reproduced with permission.[233] Copyright 2022, Wiley-VCH. c) i: Humidity sensing for hands approaching. ii: Pressure sensing for hands touching. iii: Schematic illustration showing diverse device applications. iv: Detecting various knee crook levels. v: Detecting various breath speeds. Reproduced with permission.[234] Copyright 2019, American Chemical Society.

sensing capabilities. It can detect both proximity and touch states based on humidity and pressure sensing. Additionally, the sensor can be used for detecting respiratory conditions and human joint movements by utilizing humidity and pressure sensing, making it suitable for wearable health monitoring devices. Guo and co-workers[235] developed an ultrathin breathable tactile sensor utilizing an integrated network of nanofibers by using electrospinning and spray drying techniques to directly inkjet print conductive Co_3O_4 microspheres/PEDOT:PSS/AgNW electrodes on both sides of an ionic liquid/TPU fabric electrolyte pad. The highly porous nanofiber network provided the sensor with excellent breathability and moisture permeability, ensuring long-term wear comfort. The overall thickness of the sensor was only 40 μm, allowing it to conform to any curved surface. The Co_3O_4 microspheres distributed within the nanofibers contribute to the sensor's high sensitivity of 79.5 kPa^{-1}, rapid response time of 40 ms, and wide detection range of 38 kPa, thanks to their high pseudocapacitance and microstructure. This sensor was capable of monitoring forearm swings and elbow bending, enabling quantitative detection of joint bending angles and angular frequencies. It exhibited stable and repeatable sensing signals even during repetitive movements such as stomping and continuous elbow bending, as demonstrated by 1000 repeated tests.

4.2. Sliding Detection

In the field of tactile sensing, the perception mechanisms, sensing materials, information acquisition, and practical applications of pressure sensors have been well-developed. However, due to the limitations in structure complexity, restricted fabrication technique, and unclear sliding principles, research on another crucial aspect of tactile sensing, sliding sensors, is very limited. Tactile perception of sliding includes the ability to perceive relative sliding motion at interfaces and the magnitude of shear forces on interface surfaces. By employing interlocking

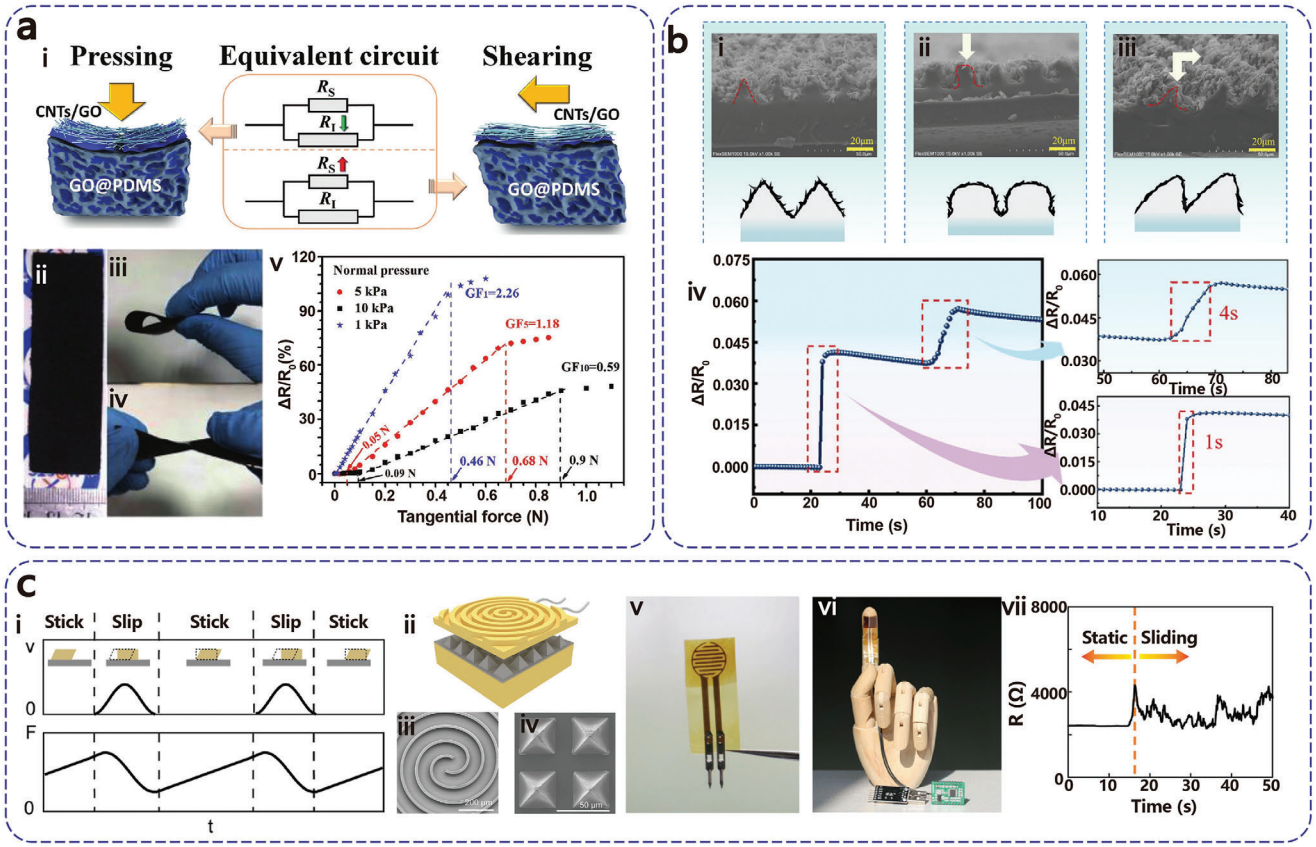

Figure 13. Sensors for sliding detection. a) i: Schematic diagram of the device under normal force or shear force. ii–iv: Photos of the sensor without and with bending or twisting. v: Resistance change under various shear forces. Reproduced with permission.[236] Copyright 2018, Wiley-VCH. b) i–iii: SEM image of the device without force, subjected to normal forces, subjected to normal and shear forces, respectively. iv: Sensor's response to gripping (normal force) and lifting (shear force). Reproduced with permission.[237] Copyright 2021, American Chemical Society. c) i: The detected friction and speed of the device. ii: Diagram of the fingertip-inspired sensor. iii: The top fingertip-inspired layer. iv: The down micropyramid layer. v: Image of the device. vi: Image showing the device attached to the robotic arm. vii: Real-time sensor responses transitioning from a static to a sliding state. Reproduced with permission.[238] Copyright 2022, Springer Nature.

structures between microstructures, sensors can obtain information about tangential forces at interfaces. With the high sensitivity provided by microstructures, surface vibrations resulting from relative sliding motion can be detected, enabling quantitative measurement and classification of different tactile sliding characteristics. Tactile perception of sliding is of significant importance in manipulation, control, and object recognition, and it holds great application value in various fields. Particularly in the field of robotic tactile sensing, the perception of sliding can assist robots in controlling object sliding and grasping forces, enabling more precise operations.

Zhang and co-workers[236] developed a flexible and stretchable piezoresistive tactile sensor by attaching two layers of CNTs/GO hybrid electrodes onto a porous PDMS layer prepared using GO-wrapped NaCl (**Figure 13a**). This sensor was capable of detecting normal and tangential forces simultaneously. The resistance decreased under normal forces and increased under tangential forces, allowing for easy differentiation of resistance changes as output. The sensor exhibited excellent sensitivity to tangential forces and showed strong consistency when subjected to stretching, bending, and shearing movements. It could also detect subtle signals generated by relative sliding as small as a feather grazing the surface. Sun and co-workers[237] constructed superhydrophobic piezoresistive tactile sensors with layered wrinkled microstructured surfaces with curled graphene nanosheets using 40 µm thick pre-stretched ultrathin medical tape (Figure 13b). The sensor differentiated normal and shear forces by distinguishing their response times. It exhibits high sensitivity, low detection limits (15 Pa for normal force and 6.4 mN for shear force), and good robustness. Based on these characteristics, the tactile sensor could monitor the real-time and accurate motion of a robotic arm during object manipulation, such as movement, grasping, and lifting. The superhydrophobicity also allowed the sensor to monitor the motion of an underwater robotic arm in real time. Zhang and co-workers[238] developed a piezoresistive tactile sensor capable of detecting slip using a combination of micropyramid structures and dual-helix microstructures that mimicked human fingerprints (Figure 13c). This sensor exhibited a high sensitivity of 11570.9 Ω/N under low forces. By integrating the tactile sensor with a readout circuit and a machine learning module, sensory signals could be effectively classified using machine learning algorithms to distinguish small pressure, large pressure, and slip signals. The sensing system based on this strategy could be installed on robot fingers, achieving a 97.4% accuracy in detecting

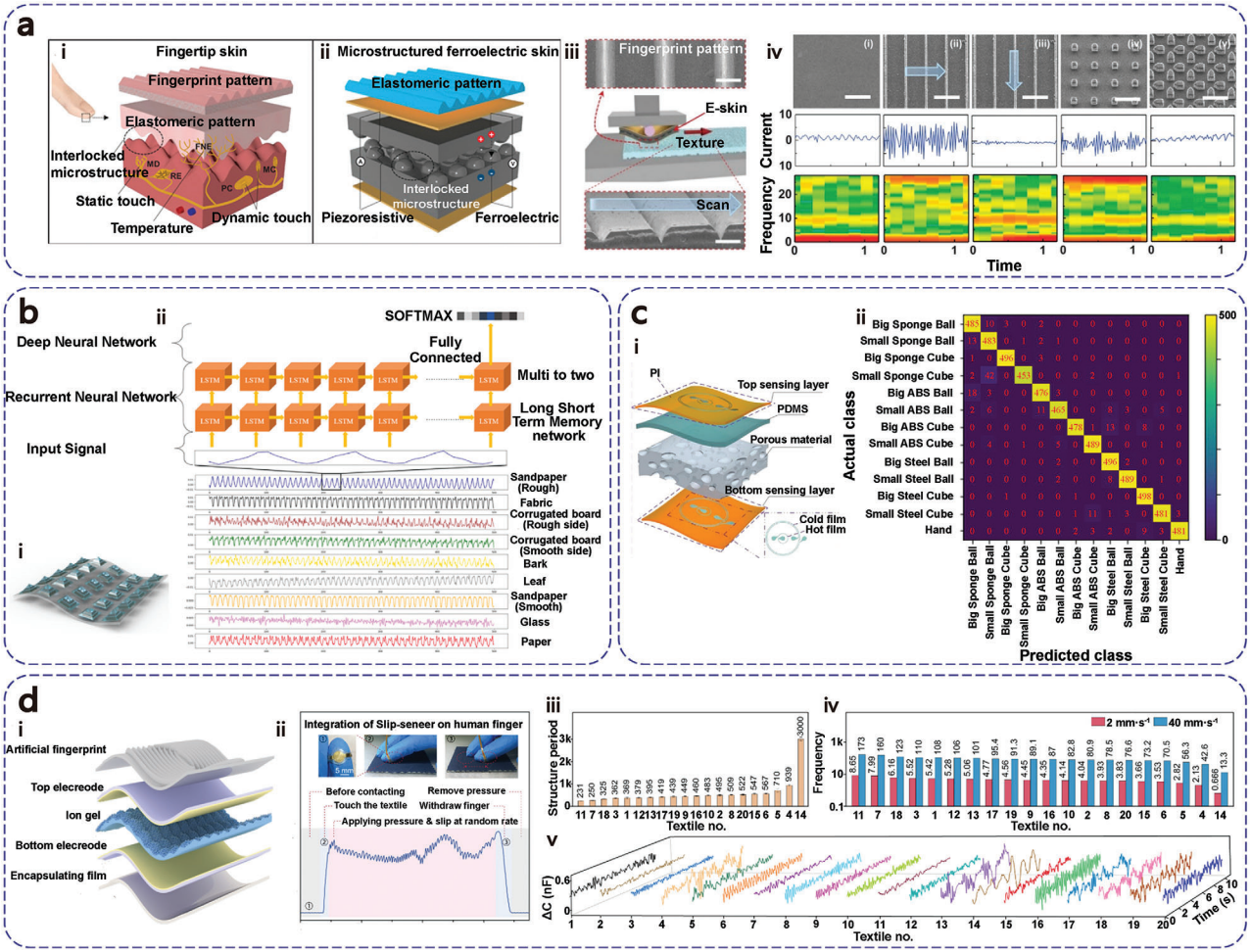

Figure 14. Sensors for roughness perception. a) i: Characteristics of human fingertips. ii: Flexible and multimodal ferroelectric sensor. iii: Schematic illustration of the sensor with interlocked microdome array. iv: Schematic illustration of texture perception measurements. v: Discrimination of various textures including SEM images, output current signals and STFT signal of various substrates. Reproduced with permission.[239] Copyright 2015, AAAS. b) i: Schematic diagram of the sensor. ii: Texture Classification architecture from electric signal during rubbing on the texture with the sensor. Reproduced with permission.[240] Copyright 2019, Springer Nature. c) i: Detailed structure of the sensor. ii: Confusion matrix for the classification test. Reproduced with permission.[241] Copyright 2020, AAAS. d) i: Diagram of the structure of the device. ii: Steps during slip detection iii: Periods of the structures for the 20 textiles. iv: Characteristic frequencies at various sliding speeds of 2 and 40 mm s^{-1}. v: Time-domain signals of 20 textiles at sliding speeds of 2 mm s^{-1}. Reproduced with permission.[242] Copyright 2023, Springer Nature.

slip and enabling precise control of the robot hand's gripping capabilities like grasping a lightweight paper cup using the robot fingertips without damaging in the presence of disturbances.

4.3. Roughness Perception

Texture roughness refers to the subtle undulations and irregularities in the surface of an object. Traditional tactile sensors are often limited by rigid structures and limited sensitivity, making it difficult to accurately perceive and quantify texture roughness. The flexible tactile sensor with microstructure has the characteristics of softness, deformability, and high sensitivity, which can obtain texture information by measuring the small deformation and pressure distribution of the object surface and accurately record the vibration spectrum information of the sensor passing through the object surface to achieve high-precision quantitative measurement and classification of different texture roughness. This type of sensor provides important tactile feedback and decision-making for tasks such as autonomous operation, object recognition, and surface quality inspection of robots.

Gao and co-workers[239] mimicked structures and functions of the human fingertip tactile system by using a combination of PVDF and rGO to create an interlocked microsphere array and utilized its piezoresistive response, piezoelectric response, and pyroelectric responses of ferroelectric polymers to develop a multimodal flexible sensor capable of simultaneously detecting pressure and temperature changes (**Figure 14a**). The sensor surface used parallel ridges to amplify vibrations caused by texture, and periodic peaks in the current can be observed and transformed into FFT spectra by scanning the surface's regular topological features, enabling the perception of diverse surface textures characterized by varying topological patterns, roughness levels, and hardness. Jeon and co-workers[240] developed

a fully transparent and flexible pressure sensor by embedding ITO film into a micropyramid plastic substrate (Figure 14b). The sensor exhibited excellent sensitivity and mechanical stability within the range of 0–10 kPa and could different material textures using machine learning algorithms such as convolutional neural networks and recurrent neural networks. Zhu and co-workers[241] integrated temperature sensors on both surfaces of a microporous piezoresistive layer, resulting in a four-fold tactile sensor with the capability to sense pressure, material thermal conductivity, object temperature, and ambient temperature (Figure 14c). Through the integration of tactile sensing data with machine learning, the sensor could precisely distinguish between different shapes, sizes, and materials in a variety of objects, providing precise object recognition for robot hands. Furthermore, the intelligent hand was applied to a waste sorting task, achieving a 94% classification accuracy in identifying seven types of garbage. Guo and co-workers[242] reported a high-performance texture recognition real-time artificial sensing system based on a single high-resolution piezocapacitive tactile sensor using spatiotemporal resolution as a criterion to correlate sensing performance with recognition ability (Figure 14d). The sensor could respond to static with ultrahigh sensitivity of 519 kPa^{-1} and dynamic stimuli from 0 to 400 Hz with a high-frequency resolution of 0.02 Hz at 400 Hz, allowing precise differentiation of subtle surface characteristics. The sensory system embedded in the fingertip of the robotic arm successfully identified 20 distinct types of textiles with 100.0% accuracy at a consistent sliding rate and 98.9% accuracy at a variable sliding rate.

5. Conclusion and Prospect

This review explains the necessity of developing microstructured flexible tactile sensors and briefly introduces the working principles, advantages, and disadvantages of different materials for designing electrode layers, encapsulation layers, and active layers of sensors. After that, this review detailed explains tactile sensors with micropyramids, microhemispheres, micropillars, microporous, microcracks, topological interconnections, multilevel, random roughness, animal and plant bionic microstructures, and their representative works. The improvement of microstructures on sensing performance was discussed by analyzing the improvement of sensitivity, response time, response range, linearity range, and mechanical stability after the introduction of microstructures. Finally, this paper summarizes the application of flexible tactile sensors based on multiple template methods in large-scale tactile sensing arrays, as well as their applications in intelligent scenarios such as physiological signal detection, sliding detection, and roughness perceptions.

As mentioned in this review, the design of specific microstructures and the replication and imitation of certain microstructures found in nature have greatly expanded and improved the performance and application scenarios of tactile sensors in recent years. Nevertheless, it is important to highlight that despite these advancements, most tactile sensors are still in the early stages of development and still face great challenges in terms of multifunctional, systematic, integrated, and intelligent, especially in the following aspects.

5.1. Further Enhancement of Sensor Performance

Although better performance of tactile sensors can be achieved by microstructure designing, each type of sensor has its inherent drawbacks, making it difficult to excel in sensitivity, response time, response range, linearity range, and mechanical stability simultaneously. Sensors with micropyramid and microhemisphere structures exhibit higher sensitivity and linearity in the low-pressure range, but their sensitivity and linearity decrease significantly in the high-pressure range. Sensors with micropillar structures often have good linearity due to their uniform structure, but sensitivity is often low. Sensors with microporous structures have lower modulus and better flexibility, but their mechanical stability is poorer. Microcrack structures require complicated structural design and controlled crack formation to contribute to performance enhancement. Replica molding of natural materials often depends on the properties of the natural materials themselves, making further design and optimization difficult. Biomaterials with internal natural structures have been used in some sensors, but their poor stability makes them unsuitable for direct sensor fabrication. Some biomimetic structure sensors have been developed, but their geometric and material properties have not been deeply studied yet. The current microstructure fabrication techniques are either too complex or too costly to achieve large-scale production. Therefore, one of the challenges for researchers in the future is how to organically integrate various advantages of microstructures to enhance sensitivity, response time, response range, linearity range, durability, flexibility, and stretchability under these limitations.

5.2. Fabrication of Larger Scale and Arrayed Sensors

The superior performance of microstructured flexible tactile sensors has expanded the application scenarios for flexible tactile sensors. However, recent research has mostly focused on single-pixel devices rather than large-area, arrayed devices which are required in many application scenarios. Currently, microstructured flexible tactile sensors are mainly fabricated using a template method, which has the advantages of controllable morphology and regular arrays but is difficult to ensure the quality of morphology under large-area replication, making large-scale production hardly achievable. In addition, the current array integration based on micro-structured devices has a low integration level, generally only having a few tens of pixels. In order to achieve high-density, high integration, and low crosstalk micro/nano-scale sensor arrays, a series of simple and morphology-quality-guaranteed microstructure fabrication techniques compatible with large-area, high-density applications need to be developed, thus facilitating their application in cutting-edge fields such as large-area machine tactile perception.

5.3. Integration and Development of the Backend and Integration with Other Sensors

A complete tactile sensing system includes tactile sensing, transmission, processing, memory, and feedback systems. The keynote of the system is ensuring a dependable and consistent

data transmission, processing, and feedback network between multiple devices. Therefore, despite sensor development, the backend data processing and transmission module are equally important, including the integration of wearable wireless transmission devices and the development of machine learning algorithms for tactile recognition. Furthermore, whether the sensor is used for machine touch or wearable devices, both application scenarios face the integration with other sensors such as temperature, humidity, and gas sensors, making inevitable the interference among multiple stimuli. Therefore, how to integrate with other electronic devices on flexible substrates to develop a fully functional machine sensing system and multifunctional wearable devices, while avoiding mutual interference of different stimulus signals, is also a problem that researchers need to address.

5.4. Breathability, Biocompatibility, and Stability as Wearable Devices

For wearable tactile sensors, the sensors should also possess breathability and biocompatibility to ensure that they do not obstruct the physiological activities of the skin or organs despite mechanical flexibility. Otherwise, the sensors may interfere with sweating or respiration, making them unsuitable for continuous and long-term use. Therefore, sensors based on materials like PDMS are difficult to use as long-term wearable devices, while devices incorporating porous active layers and electrospun electrodes have the potential to address this issue. Additionally, environmental factors in everyday tasks like humidity, sweat, and water infiltration can also play a crucial role in diminishing performance over extended periods of use. Therefore, consideration should be given to the chemical and environmental robustness of the human–machine interaction system, along with biocompatible packaging technologies when designing such a system.

Acknowledgements

The authors thank the support of Natural Science Foundation of Beijing (L223006 and 2222088), National Natural Science Foundation of China (No. 52203307, 52125205, U20A20166, 61805015, 61804011, 52202181 and 52102184), the National Key R&D Program of China (2021YFB3200302 and 2021YFB3200304), the Shenzhen Science and Technology Program (KQTD20170810105439418) and the Fundamental Research Funds for the Central Universities for their support.

Conflict of Interest

The authors declare no conflict of interest.

Keywords

flexible sensors, microstructures, sensitivity, tactile sensors, wearable devices

Received: April 3, 2024
Revised: April 19, 2024
Published online:

[1] C. Xu, S. A. Solomon, W. Gao, *Nat. Mach. Intell.* **2023**, *5*, 1344.
[2] Y. Wang, M. L. Adam, Y. Zhao, W. Zheng, L. Gao, Z. Yin, H. Zhao, *Nano-Micro Lett.* **2023**, *15*, 55.
[3] B. Shih, D. Shah, J. Li, T. G. Thuruthel, Y.-L. Park, F. Iida, Z. Bao, R. Kramer-Bottiglio, M. T. Tolley, *Sci. Rob.* **2020**, *5*, eaaz9239.
[4] Z. Shi, L. Meng, X. Shi, H. Li, J. Zhang, Q. Sun, X. Liu, J. Chen, S. Liu, *Nano-Micro Lett.* **2022**, *14*, 141.
[5] D. Wang, X. Chen, G. Yuan, Y. Jia, Y. Wang, A. Mumtaz, Y. Wang, J.-M. Liu, *J. Materiomics* **2019**, *5*, 66.
[6] J. Tao, M. Dong, L. Li, C. Wang, J. Li, Y. Liu, R. Bao, C. Pan, *Microsyst. Nanoeng.* **2020**, *6*, 62.
[7] R. Bao, J. Tao, J. Zhao, M. Dong, J. Li, C. Pan, *Sci. Bull.* **2023**, *68*, 1027.
[8] F. Liu, S. Deswal, A. Christou, Y. Sandamirskaya, M. Kaboli, R. Dahiya, *Sci. Rob.* **2022**, *7*, eabl7344.
[9] Y. Shi, Z. Zhang, Q. Huang, Y. Lin, Z. Zheng, *J. Semicond.* **2023**, *44*, 021601.
[10] Q. Zhang, R. Yang, Q. Duan, Y. Zhao, Z. Qian, D. Luo, Z. Liu, R. Wang, *Chem. Eng. J.* **2024**, *482*, 148491.
[11] B. C. K. Tee, A. Chortos, A. Berndt, A. K. Nguyen, A. Tom, A. McGuire, Z. C. Lin, K. Tien, W.-G. Bae, H. Wang, P. Mei, H.-H. Chou, B. Cui, K. Deisseroth, T. N. Ng, Z. Bao, *Science* **2015**, *350*, 313.
[12] T. Kim, I. Hong, M. Kim, S. Im, Y. Roh, C. Kim, J. Lim, D. Kim, J. Park, S. Lee, D. Lim, J. Cho, S. Huh, S.-U. Jo, C. Kim, J.-S. Koh, S. Han, D. Kang, *Npj Flexible Electron.* **2023**, *7*, 22.
[13] Q. Hua, J. Sun, H. Liu, R. Bao, R. Yu, J. Zhai, C. Pan, Z. L. Wang, *Nat. Commun.* **2018**, *9*, 244.
[14] C. B. Cooper, S. E. Root, L. Michalek, S. Wu, J.-C. Lai, M. Khatib, S. T. Oyakhire, R. Zhao, J. Qin, Z. Bao, *Science* **2023**, *380*, 935.
[15] K. Yao, J. Zhou, Q. Huang, M. Wu, C. K. Yiu, J. Li, X. Huang, D. Li, J. Su, S. Hou, Y. Liu, Y. Huang, Z. Tian, J. Li, H. Li, R. Shi, B. Zhang, J. Zhu, T. H. Wong, H. Jia, Z. Gao, Y. Gao, Y. Zhou, W. Park, E. Song, M. Han, H. Zhang, J. Yu, L. Wang, W. J. Li, et al., *Nat. Mach. Intell.* **2022**, *4*, 893.
[16] Y. Zhu, Y. Li, D. Xie, B. Yan, Y. Wu, Y. Zhang, G. Wang, L. Lai, Y. Sun, Z. Yang, G. Ding, *Nano Energy* **2023**, *117*, 108862.
[17] H. Choi, U. Jeong, *Adv. Mater.* **2023**, *35*, 2306795.
[18] J. Hu, Y. Qiu, X. Wang, L. Jiang, X. Lu, M. Li, Z. Wang, K. Pang, Y. Tian, W. Zhang, Z. Xu, H. Zhang, H. Qi, A. Liu, Z. Zhang, H. Wu, *Nano Energy* **2022**, *96*, 107073.
[19] H. Qiao, S. Sun, P. Wu, *Adv. Mater.* **2023**, *35*, 2300593.
[20] J. Huang, A. Chen, J. Liao, S. Han, Q. Wu, J. Zhang, Y. Chen, X. Lin, L. Guan, *Mater. Horiz.* **2024**, *11*, 822.
[21] S. Zhao, W. Ran, L. Wang, G. Shen, *J. Semicond.* **2022**, *43*, 082601.
[22] C. Wang, L. Dong, D. Peng, C. Pan, *Adv. Intell. Syst.* **2019**, *1*, 1900090.
[23] X. Liu, Y. Yao, J. Ma, Y. Zhang, Q. Wang, Z. Zhang, T. Ren, *J. Semicond.* **2015**, *36*, 064009.
[24] H. Zhang, Y. Hong, B. Ge, T. Liang, J. Xiong, *J. Semicond.* **2013**, *34*, 125006.
[25] D. Liu, N. Mei, Z. Zhang, *J. Semicond.* **2014**, *35*, 105014.
[26] S. Li, T. Liang, W. Wang, Y. Hong, T. Zheng, J. Xiong, *J. Semicond.* **2015**, *36*, 014014.
[27] J. Su, X. Zhang, G. Zhou, C. Xia, W. Zhou, Q. Huang, *J. Semicond.* **2018**, *39*, 071005.
[28] X. Zhao, D. Li, Y. Yu, D. Wen, *J. Semicond.* **2017**, *38*, 074008.
[29] W. Gao, J. Huang, J. He, R. Zhou, Z. Li, Z. Chen, Y. Zhang, C. Pan, *InfoMat* **2023**, *5*, e12426.
[30] Z. Li, S. Zhang, Y. Chen, H. Ling, L. Zhao, G. Luo, X. Wang, M. C. Hartel, H. Liu, Y. Xue, R. Haghniaz, K. Lee, W. Sun, H. Kim, J. Lee, Y. Zhao, Y. Zhao, S. Emaminejad, S. Ahadian, N. Ashammakhi, M. R. Dokmeci, Z. Jiang, A. Khademhosseini, *Adv. Funct. Mater.* **2020**, *30*, 2003601.
[31] Z. Wang, L. Zhang, J. Liu, H. Jiang, C. Li, *Nanoscale* **2018**, *10*, 10691.

[32] S. A. Hasan, Y. Jung, S. Kim, C.-L. Jung, S. Oh, J. Kim, H. Lim, *Sensors* **2016**, *16*, 93.
[33] S. Wang, F. Gao, Y. Hu, S. Zhang, H. Shang, C. Ge, B. Tan, X. Zhang, J. Zhang, P. Hu, *Chem. Eng. J.* **2022**, *443*, 136446.
[34] Y. W. Choi, D. Kang, P. V. Pikhitsa, T. Lee, S. M. Kim, G. Lee, D. Tahk, M. Choi, *Sci. Rep.* **2017**, *7*, 40116.
[35] Y. Zhang, J. Yang, X. Hou, G. Li, L. Wang, N. Bai, M. Cai, L. Zhao, Y. Wang, J. Zhang, K. Chen, X. Wu, C. Yang, Y. Dai, Z. Zhang, C. F. Guo, *Nat. Commun.* **2022**, *13*, 1317.
[36] D. Geng, S. Chen, R. Chen, Y. You, C. Xiao, C. Bai, T. Luo, W. Zhou, *Adv. Mater. Technol.* **2022**, *7*, 2101031.
[37] N. Bai, L. Wang, Q. Wang, J. Deng, Y. Wang, P. Lu, J. Huang, G. Li, Y. Zhang, J. Yang, K. Xie, X. Zhao, C. F. Guo, *Nat. Commun.* **2020**, *11*, 209.
[38] C. M. Boutry, M. Negre, M. Jorda, O. Vardoulis, A. Chortos, O. Khatib, Z. Bao, *Sci. Rob.* **2018**, *3*, eaau6914.
[39] W. Cheng, X. Wang, Z. Xiong, J. Liu, Z. Liu, Y. Jin, H. Yao, T.-S. Wong, J. S. Ho, B. C. K. Tee, *Nat. Mater.* **2023**, *22*, 1352.
[40] J. He, Y. Zhang, R. Zhou, L. Meng, T. Chen, W. Mai, C. Pan, *J. Materiomics* **2020**, *6*, 86.
[41] Z.-X. Huang, L.-W. Li, Y.-Z. Huang, W.-X. Rao, H.-W. Jiang, J. Wang, H.-H. Zhang, H.-Z. He, J.-P. Qu, *Nat. Commun.* **2024**, *15*, 819.
[42] G. Prasad, X. Lin, J. Liang, Y. Yao, T. Tao, B. Liang, S.-G. Lu, *J. Materiomics* **2023**, *9*, 174.
[43] L. Persano, C. Dagdeviren, Y. Su, Y. Zhang, S. Girardo, D. Pisignano, Y. Huang, J. A. Rogers, *Nat. Commun.* **2013**, *4*, 1633.
[44] R. Ge, Q. Yu, F. Zhou, S. Liu, Y. Qin, *Nat. Commun.* **2023**, *14*, 6315.
[45] H. Jin, Y. Kim, W. Youm, Y. Min, S. Seo, C. Lim, C.-H. Hong, S. Kwon, G. Park, S. Park, H. J. Kim, *Npj Flexible Electron.* **2022**, *6*, 82.
[46] T. Vijayakanth, S. Shankar, G. Finkelstein-Zuta, S. Rencus-Lazar, S. Gilead, E. Gazit, *Chem. Soc. Rev.* **2023**, *52*, 6191.
[47] W. Gao, Y. Zhu, Y. Wang, G. Yuan, J.-M. Liu, *J. Materiomics* **2020**, *6*, 1.
[48] X. Chen, L. Luo, Z. Zeng, J. Jiao, M. Shehzad, G. Yuan, H. Luo, Y. Wang, *J. Materiomics* **2020**, *6*, 643.
[49] K. Zhou, Y. Zhao, X. Sun, Z. Yuan, G. Zheng, K. Dai, L. Mi, C. Pan, C. Liu, C. Shen, *Nano Energy* **2020**, *70*, 104546.
[50] J. He, R. Zhou, Y. Zhang, W. Gao, T. Chen, W. Mai, C. Pan, *Adv. Funct. Mater.* **2022**, *32*, 2107281.
[51] J. Yu, L. Chen, X. Hou, J. Mu, J. He, W. Geng, X. Qiao, X. Chou, *J. Materiomics* **2022**, *8*, 247.
[52] M. Zhang, S. Gong, K. Hakobyan, Z. Gao, Z. Shao, S. Peng, S. Wu, X. Hao, Z. Jiang, E. H. Wong, K. Liang, C. H. Wang, W. Cheng, J. Xu, *Adv. Sci.* **2024**, *11*, 2309006.
[53] C. Zhi, S. Shi, S. Meng, H. Wu, Y. Si, K. Zhang, S. Zhang, J. Hu, *Nano Energy* **2023**, *115*, 108734.
[54] H. Xu, J. Tao, Y. Liu, Y. Mo, R. Bao, C. Pan, *Small* **2022**, *18*, 2202477.
[55] D.-L. Wen, X. Liu, H.-T. Deng, D.-H. Sun, H.-Y. Qian, J. Brugger, X.-S. Zhang, *Nano Energy* **2019**, *66*, 104123.
[56] S. Gong, X. Zhang, X. A. Nguyen, Q. Shi, F. Lin, S. Chauhan, Z. Ge, W. Cheng, *Nat. Nanotechnol.* **2023**, *18*, 889.
[57] R. Han, Y. Liu, Y. Mo, H. Xu, Z. Yang, R. Bao, C. Pan, *Adv. Funct. Mater.* **2023**, *33*, 2305531.
[58] Z. Feng, Q. He, J. Qiu, X. Wang, Y. Lin, Y. Wu, J. Yang, *Adv. Mater. Technol.* **2023**, *8*, 2300949.
[59] Y. Park, H. Luan, K. Kwon, T. S. Chung, S. Oh, J.-Y. Yoo, G. Chung, J. Kim, S. Kim, S. S. Kwak, J. Choi, H.-P. Phan, S. Yoo, H. Jeong, J. Shin, S. M. Won, H.-J. Yoon, Y. H. Jung, J. A. Rogers, *Npj Flexible Electron.* **2024**, *8*, 6.
[60] J. Shi, Y. Dai, Y. Cheng, S. Xie, G. Li, Y. Liu, J. Wang, R. Zhang, N. Bai, M. Cai, Y. Zhang, Y. Zhan, Z. Zhang, C. Yu, C. F. Guo, *Sci. Adv.* **2023**, *9*, eadf8831.
[61] X. Qu, J. Li, Z. Han, Q. Liang, Z. Zhou, R. Xie, H. Wang, S. Chen, *ACS Nano* **2023**, *17*, 14904.
[62] Y. Zhang, Q. Liu, W. Ren, Y. Song, H. Luo, Y. Han, L. He, X. Wu, Z. Wang, *Research* **2023**, *6*, 0172.
[63] H. Ding, Z. Xin, Y. Yang, Y. Luo, K. Xia, B. Wang, Y. Sun, J. Wang, Y. Zhang, H. Wu, S. Fan, L. Zhang, K. Liu, *Adv. Funct. Mater.* **2020**, *30*, 1909616.
[64] Y. Wu, Y. Liu, Y. Zhou, Q. Man, C. Hu, W. Asghar, F. Li, Z. Yu, J. Shang, G. Liu, M. Liao, R.-W. Li, *Sci. Rob.* **2018**, *3*, eaat0429.
[65] H. Dai, C. Zhang, C. Pan, H. Hu, K. Ji, H. Sun, C. Lyu, D. Tang, T. Li, J. Fu, P. Zhao, *Adv. Mater.* **2024**, *36*, 2310145.
[66] J. Han, X. Dong, Z. Yin, S. Zhang, M. Li, Z. Zheng, M. C. Ugurlu, W. Jiang, H. Liu, M. Sitti, *Proc. Natl. Acad. Sci. USA* **2023**, *120*, 2308301120.
[67] H. Sun, G. Martius, *Sci. Rob.* **2022**, *7*, eabm0608.
[68] Z. Li, C. Li, Z. Xiong, G. Xu, Y. R. Wang, X. Tian, X. Yang, Z. Liu, Q. Zeng, R. Lin, Y. Li, J. K. W. Lee, J. S. Ho, C.-W. Qiu, *Phys. Rev. Lett.* **2023**, *130*, 227201.
[69] Z. Li, C. Li, G. Xu, W. Chen, Z. Xiong, H. Jing, J. S. Ho, C.-W. Qiu, *Sci. Adv.* **2023**, *9*, eadi0562.
[70] W. W. Lee, Y. J. Tan, H. Yao, S. Li, H. H. See, M. Hon, K. A. Ng, B. Xiong, J. S. Ho, B. C. K. Tee, *Sci. Rob.* **2019**, *4*, eaax2198.
[71] Y. Huang, L. Zhao, M. Cai, J. Zhu, L. Wang, X. Chen, Y. Zeng, L. Zhang, J. Shi, C. F. Guo, *Adv. Healthcare Mater.* **2023**, *12*, 2301838.
[72] Z. Shen, C. Yang, C. Yao, Z. Liu, X. Huang, Z. Liu, J. Mo, H. Xu, G. He, J. Tao, X. Xie, T. Hang, H.-J. Chen, F. Liu, *Mater. Horiz.* **2023**, *10*, 499.
[73] L. Ma, X. Yu, Y. Yang, Y. Hu, X. Zhang, H. Li, X. Ouyang, P. Zhu, R. Sun, C.-p. Wong, *J. Materiomics* **2020**, *6*, 321.
[74] Y. Jung, J. Gu, J. Yeo, W. Lee, H. Han, J. Choi, J.-H. Ha, J. Ahn, H. Cho, S. Ryu, I. Park, *Small* **2024**, *20*, 2303981.
[75] G. Xi, D. Zhang, M. Tang, H. Zhang, Y. Sun, Y. Zhang, H. Cai, H. Xia, D. Zhou, *Nano Res.* **2023**, *17*, 4410.
[76] D. Won, J. Bang, S. H. Choi, K. R. Pyun, S. Jeong, Y. Lee, S. H. Ko, *Chem. Rev.* **2023**, *123*, 9982.
[77] X. Pan, Z. Xu, R. Bao, C. Pan, *Adv. Sens. Res.* **2023**, *2*, 2300065.
[78] U. S. Bubniene, V. Ratautaite, A. Ramanavicius, V. Bucinskas, *Polymers* **2022**, *14*, 2984.
[79] H. H. Shi, N. Khalili, T. Morrison, H. E. Naguib, *ACS Appl. Mater. Interfaces* **2018**, *10*, 19037.
[80] Z. Li, K. Zhao, J. Wang, B. Wang, J. Lu, B. Jia, T. Ji, X. Han, G. Luo, Y. Yu, L. Wang, M. Li, Z. Wang, L. Zhao, *ACS Appl. Mater. Interfaces* **2024**, *16*, 7384.
[81] M. Saidi, A. Beldjilali, N. Saidi-Amroun, *Adv. Mater. Res.* **2011**, *324*, 328.
[82] X. Lin, T. Zhang, J. Cao, H. Wen, T. Fei, S. Liu, R. Wang, H. Ren, H. Zhao, *J. Bionic Eng.* **2020**, *17*, 55.
[83] Y. Wan, J. Tao, M. Dong, L. Zhang, Z. Peng, R. Bao, C. Pan, *Adv. Mater. Technol.* **2022**, *7*, 2200386.
[84] L. Wang, X. Xu, J. Chen, W. Su, F. Zhang, A. Li, C. Li, C. Xu, Y. Sun, *ACS Nano* **2022**, *16*, 12645.
[85] J. Zhang, H. Yao, J. Mo, S. Chen, Y. Xie, S. Ma, R. Chen, T. Luo, W. Ling, L. Qin, Z. Wang, W. Zhou, *Nat. Commun.* **2022**, *13*, 5076.
[86] Y. Hou, L. Wang, R. Sun, Y. Zhang, M. Gu, Y. Zhu, Y. Tong, X. Liu, Z. Wang, J. Xia, Y. Hu, L. Wei, C. Yang, M. Chen, *ACS Nano* **2022**, *16*, 8358.
[87] C. Chen, J.-L. Xu, Q. Wang, X.-L. Li, F.-Q. Xu, Y.-C. Gao, Y.-B. Zhu, H.-A. Wu, J.-W. Liu, *Adv. Mater.* **2024**, *36*, 2313228.
[88] J. Li, S. Li, Y. Su, *Adv. Funct. Mater.* **2022**, *32*, 2208216.
[89] S. Chen, S. Li, S. Peng, Y. Huang, J. Zhao, W. Tang, X. Guo, *J. Semicond.* **2018**, *39*, 013001.
[90] C. Zhang, W. Ouyang, L. Zhang, D. Li, *Microsyst. Nanoeng.* **2023**, *9*, 158.
[91] A. Miyamoto, S. Lee, N. F. Cooray, S. Lee, M. Mori, N. Matsuhisa, H. Jin, L. Yoda, T. Yokota, A. Itoh, M. Sekino, H. Kawasaki, T. Ebihara, M. Amagai, T. Someya, *Nat. Nanotechnol.* **2017**, *12*, 907.

[92] C. Zhang, Q. Yang, X. Meng, H. Li, Z. Luo, L. Kai, J. Liang, S. Chen, F. Chen, *Adv. Sci.* **2023**, *10*, 2303418.
[93] S. Nam, C. Park, S.-H. Sunwoo, M. Kim, H. Lee, M. Lee, D.-H. Kim, *Soft Sci.* **2023**, *3*, 28.
[94] T. Kim, A. H. Kalhori, T.-H. Kim, C. Bao, W. S. Kim, *Microsyst. Nanoeng.* **2022**, *8*, 120.
[95] X. Li, Y. Lin, L. Cui, C. Li, Z. Yang, S. Zhao, T. Hao, G. Wang, J.-Y. Heo, J.-C. Yu, Y.-W. Chang, J. Zhu, *ACS Appl. Mater. Interfaces* **2023**, *15*, 56233.
[96] Y. Sekertekin, I. Bozyel, D. Gokcen, *Sensors* **2020**, *20*, 2908.
[97] H. Devaraj, R. Schober, M. Picard, M. Y. Teo, C.-Y. Lo, W. C. Gan, K. C. Aw, *Measurement: Sensors* **2019**, *2–4*, 100004.
[98] H. Kong, Z. Song, W. Li, Y. Bao, D. Qu, Y. Ma, Z. Liu, W. Wang, Z. Wang, D. Han, L. Niu, *ACS Nano* **2021**, *15*, 16218.
[99] Y.-T. Niu, F.-Z. Qing, X.-S. Li, B. Peng, *Rare Met.* **2022**, *41*, 1727.
[100] W. Wang, Y. Jiang, D. Zhong, Z. Zhang, S. Choudhury, J.-C. Lai, H. Gong, S. Niu, X. Yan, Y. Zheng, C.-C. Shih, R. Ning, Q. Lin, D. Li, Y.-H. Kim, J. Kim, Y.-X. Wang, C. Zhao, C. Xu, X. Ji, Y. Nishio, H. Lyu, J. B. H. Tok, Z. Bao, *Science* **2023**, *380*, 735.
[101] S. Park, H. Kim, M. Vosgueritchian, S. Cheon, H. Kim, J. H. Koo, T. R. Kim, S. Lee, G. Schwartz, H. Chang, Z. Bao, *Adv. Mater.* **2014**, *26*, 7324.
[102] D. Xie, Q. Jiang, G. Fu, Y. Ding, X. Kang, W. Cao, Y. Zhao, *Rare Met.* **2011**, *30*, 94.
[103] B. Huang, Q. Jiang, H. Chen, L. He, X. Li, G. Fu, Y. Zhao, *Rare Met.* **2011**, *30*, 98.
[104] N. Dai, X. Guan, C. Lu, K. Zhang, S. Xu, I. M. Lei, G. Li, Q. Zhong, P. Fang, J. Zhong, *ACS Nano* **2023**, *17*, 24814.
[105] W. Tang, X. Weng, Y. Wu, L. Deng, *Rare Met.* **2006**, *25*, 65.
[106] R. Qin, J. Nong, K. Wang, Y. Liu, S. Zhou, M. Hu, H. Zhao, G. Shan, *Adv. Mater.* **2024**, *36*, 2312761.
[107] Y. Song, R. Y. Tay, J. Li, C. Xu, J. Min, E. Shirzaei Sani, G. Kim, W. Heng, I. Kim, W. Gao, *Sci. Adv.* **2023**, *9*, eadi6492.
[108] B. Wang, W. Zhang, C. Lai, Y. Liu, H. Guo, D. Zhang, Z. Guo, *Small* **2023**, *19*, 2302335.
[109] J. Jia, Y. Zhu, P. Das, J. Ma, S. Wang, G. Zhu, Z.-S. Wu, *J. Materiomics* **2023**, *9*, 1242.
[110] Z. Cai, Y.-F. Ma, M. Wang, A. N. Qian, Z.-M. Tong, L.-T. Xiao, S.-T. Jia, X.-Y. Chen, *Rare Met.* **2022**, *41*, 2084.
[111] L.-Y. Xiu, Z.-Y. Wang, J.-S. Qiu, *Rare Met.* **2020**, *39*, 1237.
[112] Q.-Q. Xiong, T. Muhmood, C.-X. Zhao, J.-S. Xu, X.-F. Yang, *Rare Met.* **2023**, *42*, 1175.
[113] K. Zhou, C. Zhang, Z. Xiong, H.-Y. Chen, T. Li, G. Ding, B. Yang, Q. Liao, Y. Zhou, S.-T. Han, *Adv. Funct. Mater.* **2020**, *30*, 2001296.
[114] S.-K. Le, Q.-J. Jin, J.-A. Han, H.-C. Zhou, Q.-S. Liu, F. Yang, J. Miao, P.-P. Liu, C.-Z. Zhu, H.-T. Xu, *Rare Met.* **2024**, *43*, 1390.
[115] X. He, Z. Cui, F. Zhang, Y. Li, J. Tu, J. Cao, J. Wang, Y. Qiao, P. Xi, T. Xu, X. Chen, X. Zhang, *ACS Nano* **2024**, *18*, 8296.
[116] Y. Liu, J. Tao, Y. Mo, R. Bao, C. Pan, *Adv. Mater.* **2024**, *36*, 2313857.
[117] W. Guo, Z. Ma, Z. Chen, H. Hua, D. Wang, M. Elhousseini Hilal, Y. Fu, P. Lu, J. Lu, Y. Zhang, D. Ho, B. L. Khoo, *Chem. Eng. J.* **2024**, *485*, 149659.
[118] T. An, Y. Zhang, J. Wen, Z. Dong, Q. Du, L. Liu, Y. Wang, G. Xing, X. Zhao, *ACS Sens.* **2024**, *9*, 726.
[119] Y. Wang, H. Qin, Z. Li, J. Dai, H.-P. Cong, S.-H. Yu, *Nat. Synth.* **2022**, *1*, 975.
[120] J. Lv, G. Thangavel, Y. Xin, D. Gao, W. C. Poh, S. Chen, P. S. Lee, *Nat. Commun.* **2023**, *14*, 7132.
[121] M. Jiang, H. Hu, C. Jin, R. Lv, J. Guo, S. Jiang, Z. Bai, *ACS Appl. Mater. Interfaces* **2023**, *15*, 55009.
[122] X.-H. Zhao, Q.-T. Lai, W.-T. Guo, Z.-H. Liang, Z. Tang, X.-G. Tang, V. A. L. Roy, Q.-J. Sun, *ACS Appl. Mater. Interfaces* **2023**, *15*, 30486.
[123] F.-L. Gao, J. Liu, X.-P. Li, Q. Ma, T. Zhang, Z.-Z. Yu, J. Shang, R.-W. Li, X. Li, *ACS Nano* **2023**, *17*, 16036.
[124] L. Wen, M. Nie, J. Fan, P. Chen, B. Li, S. Chen, Y. Xiong, Q. Zhang, K. Yin, L. Sun, *Adv. Intell. Syst.* **2023**, *5*, 2300337.
[125] S. Gong, W. Schwalb, Y. Wang, Y. Chen, Y. Tang, J. Si, B. Shirinzadeh, W. Cheng, *Nat. Commun.* **2014**, *5*, 3132.
[126] M. Lei, K. Feng, S. Ding, M. Wang, Z. Dai, R. Liu, Y. Gao, Y. Zhou, Q. Xu, B. Zhou, *ACS Nano* **2022**, *16*, 12620.
[127] X. Wang, Y. Gu, Z. Xiong, Z. Cui, T. Zhang, *Adv. Mater.* **2014**, *26*, 1336.
[128] X. Zhang, Z. Li, C. Liu, J. Shan, X. Guo, X. Zhao, J. Ding, H. Yang, *J. Materiomics* **2024**, *10*, 7.
[129] H.-W. Zhou, C. Zhao, Z.-Y. Zhao, J.-C. Jiang, H.-L. Jin, S. Wang, S. Pan, M.-Y. Xu, Y.-H. Chen, H.-M. Jin, *Rare Met.* **2024**, *43*, 1186.
[130] S. El-Molla, A. Albrecht, E. Cagatay, P. Mittendorfer, G. Cheng, P. Lugli, J. F. Salmerón, A. Rivadeneyra, *J. Sens.* **2016**, *2016*, 1736169.
[131] G.-W. Hsieh, C.-Y. Chien, *Polymers* **2023**, *15*, 3816.
[132] M. Suzuki, T. Takahashi, S. Aoyagi, *Micromachines* **2012**, *3*, 315.
[133] F. Xu, H. Zhang, H. Liu, W. Han, Z. Nie, Y. Lu, H. Wang, J. Zhu, *Proc. Natl. Acad. Sci. USA* **2024**, *121*, 2317440121.
[134] P. Yu, X. Li, H. Li, Y. Fan, J. Cao, H. Wang, Z. Guo, X. Zhao, Z. Wang, G. Zhu, *ACS Appl. Mater. Interfaces* **2021**, *13*, 24062.
[135] J. Lin, X. Chen, P. Zhang, Y. Xue, Y. Feng, Z. Ni, Y. Tao, Y. Wang, J. Liu, *Adv. Mater.* **2024**, *36*, 2400181.
[136] C. M. Boutry, A. Nguyen, Q. O. Lawal, A. Chortos, S. Rondeau-Gagné, Z. Bao, *Adv. Mater.* **2015**, *27*, 6954.
[137] Y.-S. Chen, G.-W. Hsieh, S.-P. Chen, P.-Y. Tseng, C.-W. Wang, *ACS Appl. Mater. Interfaces* **2015**, *7*, 45.
[138] P. Wang, G. Li, J. Liu, Z. Hou, C. Meng, S. Guo, C. Liu, S. Fan, *Adv. Mater. Interfaces* **2021**, *8*, 2100998.
[139] S. Sharma, G. B. Pradhan, S. Jeong, S. Zhang, H. Song, J. Y. Park, *ACS Nano* **2023**, *17*, 8355.
[140] H. Niu, X. Wei, H. Li, F. Yin, W. Wang, R.-S. Seong, Y. K. Shin, Z. Yao, Y. Li, E.-S. Kim, N.-Y. Kim, *Adv. Sci.* **2024**, *11*, 2305528.
[141] Y.-m. Yuan, B. Liu, M. R. Adibeig, Q. Xue, C. Qin, Q.-y. Sun, Y. Jin, M. Wang, C. Yang, *Adv. Mater.* **2024**, *36*, 2310429.
[142] R. Yin, L. Li, L. Wang, Z. Lou, *J. Semicond.* **2023**, *44*, 032602.
[143] G. Sun, P. Wang, C. Meng, *Nano Energy* **2023**, *118*, 109006.
[144] S. Li, J. Huang, M. Wang, K. Deng, C. Guo, B. Li, Y. Cheng, H. Sun, H. Ye, T. Pan, Y. Chang, *Adv. Sci.* **2023**, *10*, 2304106.
[145] M. Cao, M. Leng, W. Pan, Y. Wang, S. Tan, Y. Jiao, S. Yu, S. Fan, T. Xu, T. Liu, L. Li, J. Su, *Nano Energy* **2023**, *112*, 108492.
[146] Y. Bai, L. Yin, C. Hou, Y. Zhou, F. Zhang, Z. Xu, K. Li, Y. Huang, *Adv. Funct. Mater.* **2023**, *33*, 2214119.
[147] S. Li, A. Liu, W. Qiu, Y. Wang, G. Liu, J. Liu, Y. Shi, Y. Li, J. Li, W. Cai, C. Park, M. Ye, W. Guo, *ACS Nano* **2024**, *18*, 4579.
[148] G. Sun, P. Wang, Y. Jiang, H. Sun, T. Liu, G. Li, W. Yu, C. Meng, S. Guo, *Nano Energy* **2023**, *110*, 108367.
[149] K. Kwon, J. U. Kim, S. M. Won, J. Zhao, R. Avila, H. Wang, K. S. Chun, H. Jang, K. H. Lee, J.-H. Kim, S. Yoo, Y. J. Kang, J. Kim, J. Lim, Y. Park, W. Lu, T.-i. Kim, A. Banks, Y. Huang, J. A. Rogers, *Nat. Biomed. Eng.* **2023**, *7*, 1215.
[150] C. M. Boutry, Y. Kaizawa, B. C. Schroeder, A. Chortos, A. Legrand, Z. Wang, J. Chang, P. Fox, Z. Bao, *Nat. Electron.* **2018**, *1*, 314.
[151] G. Yao, C. Yin, Q. Wang, T. Zhang, S. Chen, C. Lu, K. Zhao, W. Xu, T. Pan, M. Gao, Y. Lin, *J. Materiomics* **2020**, *6*, 397.
[152] A. Tashakori, Z. Jiang, A. Servati, S. Soltanian, H. Narayana, K. Le, C. Nakayama, C.-l. Yang, Z. J. Wang, J. J. Eng, P. Servati, *Nat. Mach. Intell.* **2024**, *6*, 106.
[153] J. Su, H. Zhang, H. Li, K. He, J. Tu, F. Zhang, Z. Liu, Z. Lv, Z. Cui, Y. Li, J. Li, L. Z. Tang, X. Chen, *Adv. Mater.* **2024**, *36*, 2311549.
[154] J. Man, Z. Jin, J. Chen, *Adv. Sci.* **2024**, *11*, 2306832.
[155] H. Zhang, D.-Z. Zhang, D.-Y. Wang, Z.-Y. Xu, Y. Yang, B. Zhang, *Rare Met.* **2022**, *41*, 3117.
[156] H. Zhao, Y. Zhang, L. Han, W. Qian, J. Wang, H. Wu, J. Li, Y. Dai, Z. Zhang, C. R. Bowen, Y. Yang, *Nano-Micro Lett.* **2023**, *16*, 11.

[157] W. Lin, Z. Wang, Y. Xu, Z. Hu, W. Zhao, Z. Zhu, Z. Sun, G. Wang, Z. Peng, *Adv. Mater.* **2024**, *36*, 2305032.
[158] Q. Ouyang, C. Yao, H. Chen, L. Song, T. Zhang, D. Chen, L. Yang, M. Chen, H.-j. Chen, Z. Peng, X. Xie, *Biosens. Bioelectron.* **2024**, *246*, 115873.
[159] S. Pyo, J. Choi, J. Kim, *Adv. Electron. Mater.* **2018**, *4*, 1700427.
[160] H. Zhu, H. Luo, M. Cai, J. Song, *Adv. Sci.* **2024**, *11*, 2307693.
[161] Z. Dong, Q. He, D. Shen, Z. Gong, D. Zhang, W. Zhang, T. Ono, Y. Jiang, *Microsyst. Nanoeng.* **2023**, *9*, 31.
[162] R. Kaveti, J. H. Lee, J. K. Youn, T.-M. Jang, W. B. Han, S. M. Yang, J.-W. Shin, G.-J. Ko, D.-J. Kim, S. Han, H. Kang, A. J. Bandodkar, H.-Y. Kim, S.-W. Hwang, *Adv. Mater.* **2024**, *36*, 2307391.
[163] Y. Liu, H. Xu, M. Dong, R. Han, J. Tao, R. Bao, C. Pan, *Adv. Mater. Technol.* **2022**, *7*, 2200504.
[164] C. Pang, J. H. Koo, A. Nguyen, J. M. Caves, M.-G. Kim, A. Chortos, K. Kim, P. J. Wang, J. B. H. Tok, Z. Bao, *Adv. Mater.* **2015**, *27*, 634.
[165] K. Shang, C. He, J. Zhou, P. Ling, X. Lu, C. Fu, Y. Zhang, C. Tang, L. Qian, T. Yang, *Chem. Eng. J.* **2023**, *475*, 146279.
[166] E. Shirzaei Sani, C. Xu, C. Wang, Y. Song, J. Min, J. Tu, S. A. Solomon, J. Li, J. L. Banks, D. G. Armstrong, W. Gao, *Sci. Adv.* **2023**, *9*, eadf7388.
[167] S. Wang, Y. Nie, H. Zhu, Y. Xu, S. Cao, J. Zhang, Y. Li, J. Wang, X. Ning, D. Kong, *Sci. Adv.* **2022**, *8*, eabl5511.
[168] Y. Pang, X. Xu, S. Chen, Y. Fang, X. Shi, Y. Deng, Z.-L. Wang, C. Cao, *Nano Energy* **2022**, *96*, 107137.
[169] B. Sadri, W. Gao, *Appl. Phys. Rev.* **2023**, *10*, 031303.
[170] S. Chen, K. Hou, T. Li, X. Wu, Z. Wang, L. Wei, W. L. Leong, *Adv. Mater. Technol.* **2023**, *8*, 2200611.
[171] Y. Wu, S. Dong, X. Li, L. Wen, H. Shen, M. Li, X. Liu, Y. Zhang, G. Zeng, J. Zheng, D. Wu, *Soft Sci.* **2023**, *3*, 33.
[172] D. Lu, T. Liu, X. Meng, B. Luo, J. Yuan, Y. Liu, S. Zhang, C. Cai, C. Gao, J. Wang, S. Wang, S. Nie, *Adv. Mater.* **2023**, *35*, 2209117.
[173] S. Liu, W. Zhang, J. He, Y. Lu, Q. Wu, M. Xing, *Adv. Fiber Mater.* **2024**, *6*, 36.
[174] S. C. B. Mannsfeld, B. C. K. Tee, R. M. Stoltenberg, C. V. H. H. Chen, S. Barman, B. V. O. Muir, A. N. Sokolov, C. Reese, Z. Bao, *Nat. Mater.* **2010**, *9*, 859.
[175] S. Miller, Z. Bao, *J. Mater. Res.* **2015**, *30*, 3584.
[176] L. Pan, A. Chortos, G. Yu, Y. Wang, S. Isaacson, R. Allen, Y. Shi, R. Dauskardt, Z. Bao, *Nat. Commun.* **2014**, *5*, 3002.
[177] Z. Zhang, X. Gui, Q. Hu, L. Yang, R. Yang, B. Huang, B.-R. Yang, Z. Tang, *Adv. Electron. Mater.* **2021**, *7*, 2100174.
[178] Y.-m. Yuan, B. Liu, M. R. Adibeig, Q. Xue, C. Qin, Q.-y. Sun, Y. Jin, M. Wang, C. Yang, *Adv. Mater.* **2023**, *35*, 2310429.
[179] J.-H. Zhang, Z. Li, J. Xu, J. Li, K. Yan, W. Cheng, M. Xin, T. Zhu, J. Du, S. Chen, X. An, Z. Zhou, L. Cheng, S. Ying, J. Zhang, X. Gao, Q. Zhang, X. Jia, Y. Shi, L. Pan, *Nat. Commun.* **2022**, *13*, 5839.
[180] Q. Su, Q. Zou, Y. Li, Y. Chen, S.-Y. Teng, J. T. Kelleher, R. Nith, P. Cheng, N. Li, W. Liu, S. Dai, Y. Liu, A. Mazursky, J. Xu, L. Jin, P. Lopes, S. Wang, *Sci. Adv.* **2021**, *7*, eabi4563.
[181] R. Yang, A. Dutta, B. Li, N. Tiwari, W. Zhang, Z. Niu, Y. Gao, D. Erdely, X. Xin, T. Li, H. Cheng, *Nat. Commun.* **2023**, *14*, 2907.
[182] S. Luo, X. Zhou, X. Tang, J. Li, D. Wei, G. Tai, Z. Chen, T. Liao, J. Fu, D. Wei, J. Yang, *Nano Energy* **2021**, *80*, 105580.
[183] Y. Cao, T. Li, Y. Gu, H. Luo, S. Wang, T. Zhang, *Small* **2018**, *14*, 1703902.
[184] S. Yang, C. Zhang, J. Ji, Y. Liu, J. Wang, Z. Shi, *Adv. Mater. Technol.* **2022**, *7*, 2200309.
[185] C. Lu, Y. Gao, X. Chan, W. Yu, H. Wang, L. Hu, L. Li, *Mater. Horiz.* **2024**, *11*, 510.
[186] B. Xu, Y. Wang, H. Cui, H. Niu, Y. Liu, Z. Li, D. Chen, *Biosensors* **2022**, *12*, 506.
[187] J. Tang, C. Zhao, Q. Luo, Y. Chang, Z. Yang, T. Pan, *Npj Flexible Electron.* **2022**, *6*, 54.
[188] Z. Wang, Q. Cai, L. Lu, P. A. Levkin, *Small* **2023**, 2305214.
[189] L. Singh, K. Tripathy, M. Bhattacharjee, *Adv. Eng. Mater.* **2022**, *24*, 2200500.
[190] X. Cui, Y. Jiang, L. Hu, M. Cao, H. Xie, X. Zhang, F. Huang, Z. Xu, Y. Zhu, *Adv. Mater. Technol.* **2023**, *8*, 2200609.
[191] X. Guo, W. Hong, L. Liu, D. Wang, L. Xiang, Z. Mai, G. Tang, S. Shao, C. Jin, Q. Hong, Y. Zhao, Y. Xia, L. Yang, G. Xing, *ACS Appl. Nano Mater.* **2022**, *5*, 11028.
[192] P. Lu, L. Wang, P. Zhu, J. Huang, Y. Wang, N. Bai, Y. Wang, G. Li, J. Yang, K. Xie, J. Zhang, B. Yu, Y. Dai, C. F. Guo, *Sci. Bullet.* **2021**, *66*, 1091.
[193] P. Zhu, H. Du, X. Hou, P. Lu, L. Wang, J. Huang, N. Bai, Z. Wu, N. X. Fang, C. F. Guo, *Nat. Commun.* **2021**, *12*, 4731.
[194] T. Wang, J. Li, Y. Zhang, F. Liu, B. Zhang, Y. Wang, R. Jiang, G. Zhang, R. Sun, C.-P. Wong, *Chem. Eur. J.* **2019**, *25*, 6378.
[195] S. Kang, J. Lee, S. Lee, S. Kim, J.-K. Kim, H. Algadi, S. Al-Sayari, D.-E. Kim, D. Kim, T. Lee, *Adv. Electron. Mater.* **2016**, *2*, 1600356.
[196] M. Pruvost, W. J. Smit, C. Monteux, P. Poulin, A. Colin, *Npj Flexible Electron.* **2019**, *3*, 7.
[197] P. Wang, G. Li, W. Yu, C. Meng, S. Guo, *Adv. Electron. Mater.* **2022**, *8*, 2101269.
[198] K. Pang, X. Song, Z. Xu, X. Liu, Y. Liu, L. Zhong, Y. Peng, J. Wang, J. Zhou, F. Meng, J. Wang, C. Gao, *Sci. Adv.* **2020**, *6*, eabd4045.
[199] K.-H. Ha, W. Zhang, H. Jang, S. Kang, L. Wang, P. Tan, H. Hwang, N. Lu, *Adv. Mater.* **2021**, *33*, 2103320.
[200] Y. Guo, Z. Guo, M. Zhong, P. Wan, W. Zhang, L. Zhang, *Small* **2018**, *14*, 1803018.
[201] R. Chen, T. Luo, J. Wang, R. Wang, C. Zhang, Y. Xie, L. Qin, H. Yao, W. Zhou, *Nat. Commun.* **2023**, *14*, 6641.
[202] Y. Luo, J. Shao, S. Chen, X. Chen, H. Tian, X. Li, L. Wang, D. Wang, B. Lu, *ACS Appl. Mater. Interfaces* **2019**, *11*, 17796.
[203] B. Ji, Q. Zhou, G. Chen, Z. Dai, S. Li, Y. Xu, Y. Gao, W. Wen, B. Zhou, *J. Mater. Chem. C* **2020**, *8*, 15634.
[204] C. Wang, J. Zhao, C. Ma, J. Sun, L. Tian, X. Li, F. Li, X. Han, C. Liu, C. Shen, L. Dong, J. Yang, C. Pan, *Nano Energy* **2017**, *34*, 578.
[205] J. Li, R. Bao, J. Tao, M. Dong, Y. Zhang, S. Fu, D. Peng, C. Pan, *Appl. Phys. Rev.* **2020**, *7*, 011404.
[206] J. Zhang, T. Sun, L. Liu, S. Niu, K. Wang, H. Song, Q. Han, Z. Han, L. Ren, Q. Lin, *RSC Adv.* **2019**, *9*, 22740.
[207] H. Yao, W. Yang, W. Cheng, Y. J. Tan, H. H. See, S. Li, H. P. A. Ali, B. Z. H. Lim, Z. Liu, B. C. K. Tee, *Proc. Natl. Acad. Sci. USA* **2020**, *117*, 25352.
[208] S. Li, X. Chen, X. Li, H. Tian, C. Wang, B. Nie, J. He, J. Shao, *Sci. Adv.* **2022**, *8*, eade0720.
[209] Z. Xu, D. Wu, Z. Chen, Z. Wang, C. Cao, X. Shao, G. Zhou, S. Zhang, L. Wang, D. Sun, *Microsyst. Nanoeng.* **2023**, *9*, 5.
[210] H. Niu, H. Li, Y. Li, W. Yue, S. Gao, X. Wei, G. Shen, *Nano Energy* **2023**, *107*, 108144.
[211] J. Chen, K. Chen, J. Jin, K. Wu, Y. Wang, J. Zhang, G. Liu, J. Sun, *Nano Lett.* **2023**, *23*, 11958.
[212] J. Huang, X. Tang, F. Wang, Z. Wang, Y. Niu, H. Wang, *Adv. Eng. Mater.* **2022**, *24*, 2101767.
[213] B. Ji, Q. Zhou, M. Lei, S. Ding, Q. Song, Y. Gao, S. Li, Y. Xu, Y. Zhou, B. Zhou, *Small* **2021**, *17*, 2103312.
[214] J. Li, T. Wu, H. Jiang, Y. Chen, Q. Yang, *Adv. Intell. Syst.* **2021**, *3*, 2100070.
[215] S. Wu, C. Yang, J. Hu, M. Pan, W. Meng, Y. Liu, P. Li, J. Peng, Q. Zhang, P. Chen, H. Wang, *ACS Appl. Mater. Interfaces* **2023**, *15*, 47733.
[216] X. He, Z. Liu, G. Shen, X. He, J. Liang, Y. Zhong, T. Liang, J. He, Y. Xin, C. Zhang, D. Ye, G. Cai, *Npj Flexible Electron.* **2021**, *5*, 17.
[217] M. Yang, Y. Cheng, Y. Yue, Y. Chen, H. Gao, L. Li, B. Cai, W. Liu, Z. Wang, H. Guo, N. Liu, Y. Gao, *Adv. Sci.* **2022**, *9*, 2200507.

[218] K. Wang, Z. Lou, L. Wang, L. Zhao, S. Zhao, D. Wang, W. Han, K. Jiang, G. Shen, *ACS Nano* **2019**, *13*, 9139.
[219] K. Xia, C. Wang, M. Jian, Q. Wang, Y. Zhang, *Nano Res.* **2018**, *11*, 1124.
[220] R. S. Karmakar, C.-P. Chu, C.-L. Li, C.-H. Hsueh, Y.-C. Liao, Y.-W. Lu, *Biosensors* **2023**, *13*, 174.
[221] W. Hong, X. Guo, T. Zhang, A. Zhang, Z. Yan, X. Zhang, X. Li, Y. Guan, D. Liao, H. Lu, H. Liu, J. Hu, Y. Niu, Q. Hong, Y. Zhao, *ACS Appl. Mater. Interfaces* **2023**, *15*, 46347.
[222] T. Li, H. Luo, L. Qin, X. Wang, Z. Xiong, H. Ding, Y. Gu, Z. Liu, T. Zhang, *Small* **2016**, *12*, 5042.
[223] J. Shi, L. Wang, Z. Dai, L. Zhao, M. Du, H. Li, Y. Fang, *Small* **2018**, *14*, 1800819.
[224] Y. Wan, Z. Qiu, Y. Hong, Y. Wang, J. Zhang, Q. Liu, Z. Wu, C. F. Guo, *Adv. Electron. Mater.* **2018**, *4*, 1700586.
[225] M. Jian, K. Xia, Q. Wang, Z. Yin, H. Wang, C. Wang, H. Xie, M. Zhang, Y. Zhang, *Adv. Funct. Mater.* **2017**, *27*, 1606066.
[226] T. Yang, H. Xiang, C. Qin, Y. Liu, X. Zhao, H. Liu, H. Li, M. Ouzounian, G. Hong, H. Chen, Q. Dong, T. S. Hu, S. Liu, *Adv. Electron. Mater.* **2020**, *6*, 1900916.
[227] P. Nie, R. Wang, X. Xu, Y. Cheng, X. Wang, L. Shi, J. Sun, *ACS Appl. Mater. Interfaces* **2017**, *9*, 14911.
[228] Y. Liu, J. Tao, W. Yang, Y. Zhang, J. Li, H. Xie, R. Bao, W. Gao, C. Pan, *Small* **2022**, *18*, 2106906.
[229] F. Liu, F. Han, L. Ling, J. Li, S. Zhao, T. Zhao, X. Liang, D. Zhu, G. Zhang, R. Sun, D. Ho, C.-P. Wong, *Chem. Eur. J.* **2018**, *24*, 16823.
[230] Y. Zhang, Q. Lu, J. He, Z. Huo, R. Zhou, X. Han, M. Jia, C. Pan, Z. L. Wang, J. Zhai, *Nat. Commun.* **2023**, *14*, 1252.
[231] H. Niu, S. Gao, W. Yue, Y. Li, W. Zhou, H. Liu, *Small* **2020**, *16*, 1904774.
[232] G. Li, D. Chen, C. Li, W. Liu, H. Liu, *Adv. Sci.* **2020**, *7*, 2000154.
[233] L. Zhao, S. Yu, J. Li, Z. Song, X. Wang, *Macromol. Mater. Eng.* **2022**, *307*, 2200192.
[234] L. Miao, J. Wan, Y. Song, H. Guo, H. Chen, X. Cheng, H. Zhang, *ACS Appl. Mater. Interfaces* **2019**, *11*, 39219.
[235] P. Wang, G. Sun, W. Yu, G. Li, C. Meng, S. Guo, *Nano Energy* **2022**, *104*, 107883.
[236] C. Mu, Y. Song, W. Huang, A. Ran, R. Sun, W. Xie, H. Zhang, *Adv. Funct. Mater.* **2018**, *28*, 1707503.
[237] M. Zhang, X. Gao, C. Lu, D. Yao, L. Wu, D. Li, H. Fang, S. A., Y. Sun, *ACS Appl. Mater. Interfaces* **2021**, *13*, 55735.
[238] Y. Li, M. Zhao, Y. Yan, L. He, Y. Wang, Z. Xiong, S. Wang, Y. Bai, F. Sun, Q. Lu, Y. Wang, T. Li, T. Zhang, *Npj Flexible Electron.* **2022**, *6*, 46.
[239] J. Park, M. Kim, Y. Lee, H. S. Lee, H. Ko, *Sci. Adv.* **2015**, *1*, e1500661.
[240] M. Jung, S. K. Vishwanath, J. Kim, D.-K. Ko, M.-J. Park, S.-C. Lim, S. Jeon, *Sci. Rep.* **2019**, *9*, 14040.
[241] G. Li, S. Liu, L. Wang, R. Zhu, *Sci. Rob.* **2020**, *5*, eabc8134.
[242] N. Bai, Y. Xue, S. Chen, L. Shi, J. Shi, Y. Zhang, X. Hou, Y. Cheng, K. Huang, W. Wang, J. Zhang, Y. Liu, C. F. Guo, *Nat. Commun.* **2023**, *14*, 7121.

Guancheng Wu received his undergraduate degree from the University of Chinese Academy of Sciences in 2021. Currently, he is pursuing his Ph.D. under the supervision of Prof. Caofeng Pan at the Beijing Institute of Nanoenergy and Nanosystems, CAS. His research is mainly focused on tactile pressure sensor devices and their applications in human–machine interactions.

Rongrong Bao received her B.S. degree from Tianjin University in 2007 and her Ph.D. degree from the Technical Institute of Physics and Chemistry, Chinese Academy of Science (CAS) in 2012. She was a postdoc fellow in the same institute. She has been an Associate Professor in the group of Prof. Caofeng Pan at the Beijing Institute of Nanoenergy and Nanosystems, CAS since 2016. Her main research interests focus on the fields of the production and characterization of organic–inorganic composite nanodevices and flexible pressure sensors.

Caofeng Pan was conferred his Bachelor of Science degree in 2005 and his Ph.D. degree in 2010, both in Materials Science and Engineering, from Tsinghua University, China. Subsequently, he undertook a postdoctoral fellowship at the Georgia Institute of Technology from 2010 to 2013. In 2013, he assumed the role of a full professor at the Beijing Institute of Nanoenergy and Nanosystems, Chinese Academy of Sciences. Since 2023, he has been serving as a distinguished professor and leads a research group at the Institute of Atomic Manufacturing, Beihang University. His research endeavors predominantly focus on the exploration and application of low-dimensional materials in the development of smart wearable electronics and optoelectronic devices for tactile sensing. For further information, please visit https://www.piezotronics.cn.